INTERNSHIP REPORT

Past and future agricultural droughts: what impact of precipitation and potential evapotranspiration changes?

NON CONFIDENTIAL REPORT

Matthieu Belin

Supervised by: Aglaé Jézéquel and Agnès Ducharne

September 2024

Institut Polytechnique de Paris
M2 WAPE

Abstract

Drought is a complex phenomenon that develops across space and time. This study aimed to investigate extreme agricultural droughts in France, treating them as contiguous spatiotemporal events, and to assess their future evolution under climate change. While the mean state of the climate is expected to change, extreme dry periods are also projected to become more frequent. Consequently, drought-related damages are anticipated to increase in France by 2050. In this context, a set of high-resolution hydro-climatological simulations over France, generated during the EXPLORE2 project, was used to characterize extreme agricultural droughts both historically and under the Representative Concentration Pathway (RCP) 8.5 scenario of greenhouse gas emissions. A methodology was developed to detect and quantify these droughts as three-dimensional events. The simulations were found to reproduce extreme agricultural droughts in France comparable to those identified in the SAFRAN reanalysis. Analysis of the evolution of these extreme drought events under the RCP 8.5 scenario indicated a likely increase in their frequency and intensity. However, no significant change was observed in the median for the duration and the affected surface area of these extreme events. The most extreme droughts within each simulation exhibited the greatest changes. The attribution of these droughts to meteorological factors — precipitation and potential evapotranspiration (PET) — was also examined. Precipitation was identified as the primary meteorological factor driving extreme agricultural droughts in France, a trend that is expected to persist in the future under climate change. Additionally, a lag of two to three months was observed between an extreme precipitation deficit and the onset of an extreme agricultural drought. PET's contribution to extreme agricultural droughts is projected to increase with climate change.

Reference Teacher: Thomas Dubos
Internship Tutor: Aglaé Jézéquel and Agnès Ducharne
Internship Dates: 25/03/2024 – 16/08/2024

Declaration of Academic Integrity

Hereby I, Matthieu Belin, confirm that:

1. The results presented in this report are my own work.
2. I am the author of this report.
3. I have not used the work of others without clearly acknowledging it, and quotations and paraphrases from any source are clearly indicated.

Matthieu Belin

Rating Form

Annex 3: Rating Form

ÉCOLE POLYTECHNIQUE

RATING FORM

We wish to thank you for hosting and supervising our student for his/her research internship.

Institut Polytechnique Paris rates research internships, taking into account three elements:

- the training period
- the written report provided by the student to Ecole Polytechnique
- the defense

This form will allow the instructor to evaluate the first criterion. This evaluation form has to be completed by the host organization's internship supervisor. This evaluation should be a true representation of the intern's work, and will be taken into account for the school's official grading of student.

We would be grateful if you could fill in this form as completely as possible and email it to the instructor at Ecole Polytechnique and to the research internship coordinator:

uyen-chi.nguyen@polytechnique.edu at least one week before the defense.

NAME OF THE STUDENT : Matthieu Belin

HOST ORGANIZATION : LMD

NAME OF THE TUTOR (Scientific supervisor) : Aglaé Jézéquel

AUTONOMY	Excellent	Good	Intermediate	Weak
WORK COMMITMENT	Excellent	Good	Intermediate	Weak
INITIATIVE	Excellent	Good	Intermediate	Weak
WORK OUTCOME	Excellent	Good	Intermediate	Weak
GENERAL BEHAVIOR	Excellent	Good	Intermediate	Weak
PROFESSIONAL INTEGRATION	Excellent	Good	Intermediate	Weak
PRESENTATION OF THE WORK	Excellent	Good	Intermediate	Weak

COMMENTS :

Work quality : Matthieu est un étudiant curieux, motivé doté d'une grande capacité de travail. Il s'est très vite emparé de son sujet et possède une grande aisance avec les outils informatiques. Il a géré beaucoup de données et des outils statistiques complexes, tout en s'appuyant sur une solide base bibliographique. Il a également démontré sa capacité à contacter d'autres chercheurs.

Written report : Le rapport de Matthieu est très complet et bien documenté.

SUPERVISION OF THE INTERN

Everyday	Weekly	Monthly

Le 20/06/2024 a. jezequel

M2 WAPE
INSTITUT POLYTECHNIQUE PARIS- F 91128 PALAISEAU CEDEX

Acknowledgements

I would like to express my sincerest gratitude to my supervisors, Aglaé Jézéquel and Agnès Ducharne, for their invaluable guidance, support, and encouragement throughout my internship. Their expertise and constructive feedback have been invaluable in the development of this thesis, and their patience and dedication have contributed significantly to the quality of this internship, which has proved both enriching and rewarding.

Our discussions were always enlightening, extending beyond scientific topics and facilitating my growth both academically and personally. I am particularly grateful to Aglaé for the time she dedicated to assisting me in understanding the intricacies of academic writing, in developing this report, and in providing meticulous corrections. I would also like to express my gratitude to Agnès for encouraging me to present my work in a clear and accessible manner to a diverse audience

I would like to extend specific thanks to Jean-Philippe Vidal, Mathieu Vrac, and Lionel Guez, who offered invaluable assistance when I encountered difficulties with my data and coding challenges. Your support helped me overcome these obstacles and continue with my research.

Thanks also to all the Ph.D. students and interns who created an enjoyable place to work and grow. The informal discussions we shared and the meals we enjoyed together not only enriched my understanding of life as a Ph.D. student but also made the daily experience more rewarding and pleasant.

I am truly grateful to have had the opportunity to work under such supportive and inspiring individuals. This thesis would not have been possible without your guidance and support. Thank you for helping me navigate this academic journey with such care and commitment.

Contents

List of Figures

List of Tables

1. Introduction

Droughts are destructive natural hazards, with far-reaching consequences for biodiversity, economic activities, food production, and infrastructure on a global scale. An example is the ongoing mega-drought in Chile, which has persisted since 2010. Chile, with its Mediterranean climate and concentrated rainfall during the winter months, has a history of experiencing droughts. These droughts are driven by the El Niño Southern Oscillation (ENSO), a natural climate phenomenon. The current drought in Chile results from an interplay between natural variability including the warming of the subtropical southwest Pacific, and anthropogenic forcing, such as the increasing trend in the Southern Annular Mode due to rising greenhouse gas emissions. This situation has been further aggravated by water management practices, which have contributed to a prolonged socio-environmental crisis (Aldunce et al., 2017; Garreaud et al., 2017, 2020).

Human societies have historically developed strategies to adapt to climate variability. This has involved modifying agricultural practices, water management, and infrastructure to meet anticipated conditions. However, the low probability but high-impact nature of extreme events such as prolonged droughts represents a significant challenge. Such circumstances highlight the interdependence between climate and human society. As emphasized by the Intergovernmental Panel on Climate Change (IPCC) in its Sixth Assessment Report, extreme events have the potential to disrupt "key infrastructure and services, such as energy supply and transmission, communications, food and water supply, and transport systems in and between urban and peri-urban areas." In addition to the immediate consequences, droughts have long-term effects on ecosystems. For example, repeated drought events have caused the Amazon rainforest to shift from being a carbon sink to a net carbon source during these events due to extensive tree mortality (IPCC, 2023b).

Droughts can be defined in several ways, which reflect the complex and multifaceted nature of this phenomenon (Wilhite and Glantz, 1985). Three primary types of droughts are distinguished, depending on the place of the moisture deficit in the hydrological cycle: meteorological droughts, agricultural droughts, and hydrological droughts (IPCC, 2023a).

Meteorological droughts are characterized by an unusually low precipitation level (Wilhite and Glantz, 1985). The moisture content of the atmosphere drives this type of drought. The assessment of meteorological droughts is mainly based on two variables: total and net precipitation. Net precipitation is a function of both the total amount of precipitation and the atmospheric demand for water vapor, which is influenced by factors such as temperature and wind speed. More precisely, net precipitation is calculated as the total precipitation minus potential evapotranspiration (PET). PET is a metric representing the atmosphere's capacity to store water vapor (Raza et al., 2022). It is an estimate of the maximum possible evapotranspiration, which is the combined process of water transpiration by plants and evaporation from all surface water bodies.

The term "agricultural drought" is used to describe a situation in which there is a deficit in soil moisture (Wilhite and Glantz, 1985). This study focuses on this particular phenomenon. The direct consequences of agricultural drought include stress or death of vegetation, which can lead to biodiversity loss and a reduction in agricultural yields. It can also result in changes to soil properties, such as shrinkage and swelling in clay soils.

Hydrological droughts are defined as a deficiency in the levels of water present within natural reservoirs, including rivers, lakes, and groundwater (Wilhite and Glantz, 1985). Hydrological droughts can result in a reduction of river flow, lower water levels in surface water bodies, and diminished groundwater reserves. These droughts have significant implications for society, affecting sectors such as industry, energy production, and domestic water use.

Each type of drought impacts different economic sectors and parts of society (Wilhite and Glantz, 1985). These phenomena interact with human society through water management and land use. Droughts can also be studied as dynamic events with constant feedback between the environment and humans, defined as anthropogenic drought (AghaKouchak et al., 2021). In this study, the analysis is focused on agricultural droughts.

In metropolitan France, the effects of drought are already being observed. From 1982 to 2022, Antoni and Joassard, 2024 evaluated the annual average compensation for drought-related damages to €611 million. Droughts increase the probability of wildfires in forested regions (Barbero et al., 2019; Littell et al., 2016). Gourdier and Plat, 2018 explained that droughts also induce soil shrinkage and swelling, which can compromise the structural integrity of buildings, roads, and bridges. Moreover, the agricultural sector is significantly affected by droughts, which result in reduced crop yields and have necessitated €875 million in compensation between 2010 and 2020 alone (Tramblay et al., 2024).

Climate change introduces nonstationarity in the climate system, which in turn affects thermodynamic processes. These processes are pivotal in the development of droughts, and thus climate change may impact droughts (Seneviratne et al., 2021). The increase in the frequency of droughts due to climate change has already been observed in several drought-prone regions of the world (Clarke et al., 2022; Cook et al., 2018).

In recent years, the observed trends in drought characteristics in France have been contingent upon the specific variable employed as a drought indicator. Observed trends in France for flows remain correlated with climate variability, rather than climate change. Giuntoli et al., 2013 identified a geographic dichotomy in the trends of hydrological droughts across France. While no significant trends in low river flows were observed in the northern regions, a decrease in low flows was evident in the southern regions, including the Mediterranean coast, the Pyrenees, and the Alps. These changes are strongly correlated with large-scale climate variability phenomena, such as the North Atlantic Oscillation (NAO) and the Atlantic Multidecadal Oscillation (AMO) (Boé and Habets, 2014; Giuntoli et al., 2013). The use of precipitation data as the primary indicator revealed that France did not experience any significant trends in drought evolution during the twentieth century, as demonstrated by Lloyd-Hughes and Saunders, 2002.

Projections of climate change in France indicate that not only will average conditions become drier, but also that the frequency, intensity, and duration of extreme dry periods are likely to increase under climate change throughout the 21st century (Najac et al., 2010; Tramblay et al., 2024; Vidal et al., 2012). Roudier et al., 2016 investigated the potential impact of a projected global temperature rise of +2°C on droughts in Europe. Southern Europe including France would be vulnerable to the effects of such warming, with a marked increase (above 5%) in both the frequency and duration of hydrological drought events. France is expected to experience divergent precipitation trends across its regions. Northern France may observe an increase in precipitation, while southern France is likely to face a decrease (Marson et al., 2024; E. Sauquet et al., 2022). This north-south gradient in precipitation changes is expected to be reflected in the hydrological responses, with southern regions becoming increasingly prone to drought conditions. E. Sauquet et al., 2022 also showed that summer river flows across all French catchments are expected to decline.

From 2021 to 2024, the EXPLORE2 project was conducted in France to examine potential future scenarios for water resources and the hydrological cycle in the context of climate change (Marson et al., 2024). To this end, a high-resolution hydro-climate simulation ensemble over France was created based on the EURO-CORDEX ensemble (Jacob et al., 2014). The use of an ensemble of models to assess future changes allows for the consideration of the inherent uncertainties associated with modeling (Evin et al., 2024b).

As indicated in the report dedicated to extremes (Tramblay et al., 2024), an increase in the frequency of meteorological droughts is expected, particularly in the southern regions of France, with the summer season being the most affected. By the end of the century, there will be an increase of between 30 and 40 percent. It is projected that agricultural droughts will experience even more pronounced increases in frequency. In particular, a drought of the magnitude observed in 2022 is estimated to occur twice as often as in 2022 by the end of the century. Furthermore, the spatial extent of agricultural droughts is anticipated to expand, with an affected area three times larger than the current extent by the end of the 21st century. The frequency of these events is also expected to increase significantly by the end of the century. This trend is likely to be most pronounced during the winter months, driven by rising temperatures that exacerbate water stress in agricultural systems. Here, we focus on the most extreme droughts, to better understand the potential for record-shattering events.

The rarity and singularity of extreme events may render traditional methods of analysis and communication of results less effective, given the inherent variabilities and uncertainties between simulations. To address this challenge, an alternative approach is to utilize event-based storylines, which provide a tangible representation of plausible events (Shepherd, 2016; Sillmann et al., 2021). The methodology developed in this study provides a foundation for future analyses involving event-based storylines, offering a framework for isolating and examining specific drought events in detail. The approach focuses on the dissection of individual extreme events to understand them.

To study extreme drought events, we chose to extract droughts as spatiotemporal events. Lloyd-Hughes, 2012 argued that to accurately capture the spatio-temporal characteristics of droughts and their evolution, a three-dimensional approach must be employed, with two dimensions representing space and one representing time. By employing conventional methodologies to describe these phenomena and thereby projecting them onto a lower-order spatial and temporal space, the inherent spatio-temporal information is lost. This approach has been effectively applied in the study of other extreme events, such as heat waves (Luo et al., 2024; Vogel et al., 2020). For instance, such an approach allowed for the study of the direction of heat wave displacement (Luo et al., 2024) and the propagation of droughts within the hydrological cycle (Vidal, Martin, Franchistéguy, Habets, et al., 2010). Vidal, Martin, Franchistéguy, Habets, et al., 2010; Vidal et al., 2012 employed the analysis of three-dimensional drought events, thereby enabling the definition of specific metrics, including the mean duration of a drought event and the magnitude of the event.

The objective of this study is to analyze the most extreme drought events and their characteristics to determine the plausibility of extreme droughts at the end of the century. This report is primarily concerned with extreme drought events, which are considered to be continuous in both space and time. Additionally, it will explore the propagation of meteorological droughts into extreme agricultural droughts.

The main objective of this thesis is to examine the evolution of extreme soil drought events in France in the context of climate change. This research will establish a coherent framework for the analysis of extreme events, from their causes to their impacts. This study will examine how the most extreme soil droughts in France may evolve under changing climate conditions, with a focus on the attribution of precipitation and PET to these drought changes. By addressing these research questions, this study aims to contribute to a more comprehensive understanding of the evolution of soil droughts in France and provide insights into how climate change may influence their frequency, intensity, and impacts.

The thesis is organized as follows. The initial chapter describes the data sources and methods employed in the study. The second chapter presents the results of the analysis, which are then interpreted and discussed in the third chapter. In conclusion, the fourth chapter presents a summary of the key insights and perspectives derived from the thesis.

2. Materials and Methods

This chapter outlines the methodology employed in this study, focusing on the data sources and methods used to assess the evolution of soil droughts in metropolitan France under changing climate conditions. As mentioned in the introduction, this study concentrates on metropolitan France, and the methodology presented here can also be adapted to analyze other regions.

2.1. Data

First of all, this analysis is based on data: what are they? The data used in this analysis come from the EXPLORE2 project, which provides two main types of data: reanalysis and simulations. In both cases, data covers the same 8km × 8km grid over Metropolitan France as illustrated in Figure 2.1.

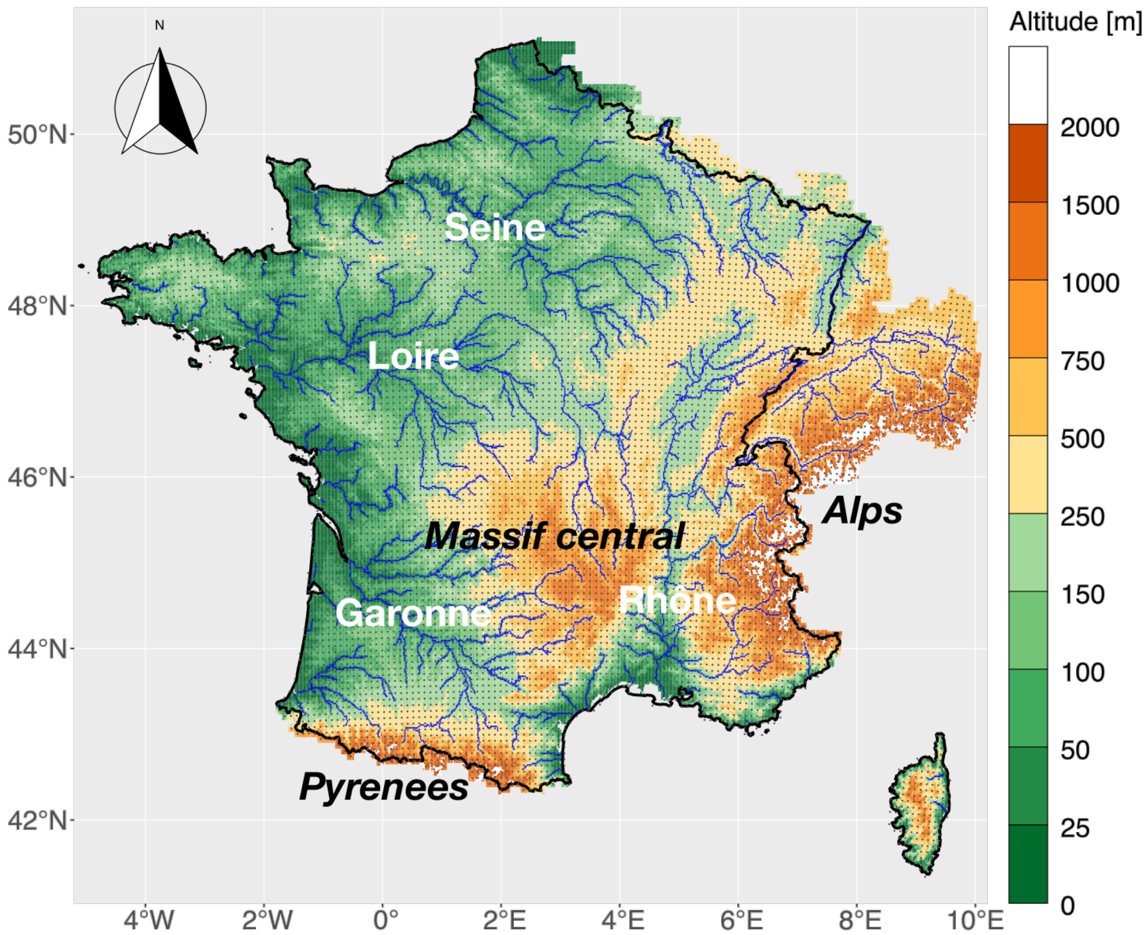

Figure 2.1 – Location of the data points.

2.1.1. Reanalysis Data

Reanalysis in climate science refers to the method of reconstructing past weather and climate conditions using a combination of historical observations and climate models. Reanalysis products offer a consistent and comprehensive dataset that can fill gaps where observational data are lacking. They permit the examination of long-term climate trends; however, they may be susceptible to biases and uncertainties, particularly in regions with limited observational data or for variables that are not directly measured.

The reanalysis data used in this project is from the SAFRAN system (Système d'Analyse Fournissant des Renseignements Atmosphériques à la Neige), a high-resolution atmospheric reanalysis developed by Météo-France. SAFRAN provides daily meteorological data on the grid shown in Figure 2.1, with records extending back to 1958 (Vidal, Martin, Franchistéguy, Baillon, and Soubeyroux, 2010). This system integrates data from numerical weather prediction models and surface observations from various networks, including both manual and automatic weather stations, to produce detailed datasets of key atmospheric variables such as temperature, precipitation, humidity, wind speed, and solar radiation (Vernay et al., 2022). SAFRAN's approach of dividing the analysis domain into climatologically homogeneous zones enhances its ability to represent local weather patterns, particularly in mountainous regions. The resulting dataset is widely used for climate monitoring, hydrological modeling, and research applications across France (Vidal, Martin, Franchistéguy, Baillon, and Soubeyroux, 2010). Hydrological data, such as soil moisture, are obtained by forcing the ORCHIDEE land-surface model (Krinner et al., 2005) with the atmospheric data from the SAFRAN reanalysis, which has been validated as a reliable source for historical data (Habets et al., 2008).

2.1.2. Simulation Data

The second type of data consists of simulations spanning from 1950 to 2100, which are generated through a series of modeling steps referred to as modeling chains. These simulations facilitate comprehension of prospective climate conditions under diverse greenhouse gas (GHG) emission scenarios.

The input data for these simulations are GHG concentration scenarios known as Representative Concentration Pathways (RCPs) (van Vuuren et al., 2011). For this study, the focus is on RCP8.5, a scenario of high GHG emissions leading to an increase in radiative forcing of +8.5 W/m^2 by 2100. This scenario serves to explore potential future droughts under severe climate change conditions if no strong enough environmental policies are implemented.

From these GHG emission scenarios, Global Climate Models (GCMs) have then been used to simulate the climate evolution globally. These models, which couple atmospheric, land, and oceanic processes, operate on a coarse grid of approximately 100 x 100 km. The Coupled Model Intercomparison Project (CMIP) aimed to create a global dataset of climate simulations over the 21st century with several GCMs (Taylor et al., 2012).

For regional studies, the CORDEX ensembles downscaled dynamically GCM's simulations on a higher resolution grid forcing Regional Climate Models (RCMs) over the region of interest (Giorgi and Jr, 2015). Simulations of the fifth phase of CMIP have been downscaled over Europe to 12 km $\times$ 12 km grid within the EURO-CORDEX ensemble. It couples different GCMs and RCMs, allowing for an evaluation of the uncertainties and specificities of each couple (Vautard et al., 2021).

Then, in the EXPLORE2 dataset, a Bias Correction method (BC) was applied to simulations of the EURO-CORDEX ensemble (Robin et al., 2023). This process aims to align the statistics of the simulated atmospheric variables with those of the reanalysis. It also ensures that the corrected atmospheric data are on the same 8 x 8 km grid as SAFRAN. Robin et al., 2023 compared three BC methods for climate variables and showed close results in terms of warming with 0.5°C of maximum differences in summer. They also showed that global projections, through the fifth and sixth phases of CMIP, simulate warmer summers and dryer winters than the corrected data. Yet, only the ADAMONT method (Verfaillie et al., 2017) using SAFRAN data from 1980 to 2011 as a reference is available for hydrological simulation. Therefore, this study uses only data corrected in bias with ADAMONT. In this analysis, precipitations and PET are computed at this step. More details about PET's calculation are provided in Appendix C.

The final step in the modeling chain involves forcing a Land Surface Model (LSM) with the corrected atmospheric data to obtain hydrological variables, particularly the soil wetness index. The EXPLORE2 project used nine LSMs and assessed their differences (É. Sauquet et al., 2023). The analysis focuses on the ORCHIDEE model outputs (Krinner et al., 2005).

In this study, soil moisture is quantified using the Soil Wetness Index (SWI) (Dirmeyer et al., 1999), defined as:

$$SWI = \frac{w_{tot} - w_{wilt}}{w_{fc} - w_{wil}} \tag{2.1}$$

where w_{tot} is the volumetric water content of a soil column, w_{wilt} is the water content at the wilting point (the minimum water content before vegetation can no longer extract it), and w_{fc} is the water content at field capacity (the maximum amount of water the soil can hold before excess water begins to drain away as runoff).

This index incorporates characteristics of both the soil and the vegetation, as well as the quantity of water present, making it particularly useful for assessing agricultural drought.

For this study, 17 of the 19 simulations were retained, with two excluded due to their temperature and precipitation projections falling outside the confidence intervals defined by the CMIP6 ensemble Marson et al., 2024. Detailed information about the models used to create this ensemble is provided in Appendix A.

In terms of temporal resolution, the data are averaged monthly to facilitate the analysis of drought patterns, which require a longer-term perspective.

To address the uncertainties inherent in climate projections, four simulations have been identified as particularly relevant in the context of the EXPLORE2 project (Marson et al., 2024). These simulations are dynamic storylines representing plausible climate scenarios in France under climate change. The objective of such storylines is to represent the variability of a simulation ensemble and the uncertainties in a comprehensible manner (Shepherd, 2019; Shepherd et al., 2018). In this report, if not specified, storylines refer to dynamic storylines, not event-based storylines. These storylines encompass different potential climate futures, providing a comprehensive view of possible scenarios:

- **Green Storyline**: Characterized by marked warming (+4.8°C on average for France at the end of the century) and increased precipitation. This scenario explores the impact of a wetter climate with higher temperatures.

- **Orange Storyline**: Marked by strong warming (+4.6°C) and drying, particularly in summer. This scenario highlights the potential for more severe drought conditions.

- **Yellow Storyline**: Features relatively little future change (+3.7°C), serving as a baseline to compare against more extreme scenarios.

- **Purple Storyline**: Characterized by strong warming (+5°C) and pronounced seasonal precipitation contrasts. This scenario examines the impact of variable precipitation patterns combined with higher temperatures.

Analyzing drought events within these storylines can provide a better understanding of the range of potential future drought conditions. More details on the models behind these storylines are provided in Appendix B.

2.2. How to Assess Moisture Deficit?

The objective is to detect droughts within the data extracted from the EXPLORE2 dataset. As previously discussed in Chapter 1, a drought is defined as a localised deficit in moisture compared to a reference period. In their review, Zargar et al., 2011 assessed six major indices for their suitability for assessing droughts. Some combined variables, such as the Palmer Drought Severity Index, which computes four terms in the water balance equation (Palmer, 1965). In regard to the assessment of droughts on specific variables, Zargar et al., 2011 outlines three methodologies: percent of normal, deciles, and standardized indices. The initial two methods are insufficiently robust (Zargar et al., 2011); however, this shortcoming is overcome by standardized indices that normalize the data before assessing surpluses or deficiencies (McKee et al., 1993). These indices have been widely adopted in research (Zargar et al., 2011) and are used in our methodology. One of the advantages of such indices is that they facilitate the comparison of values across different geographical locations and thus different climates (McKee et al., 1993).

2.2.1. Basis of Standardized Indices: Standardized Precipitation Index Calculation

Initially, standardized indices have been introduced for precipitations by McKee et al., 1993. They developed the *Standardized Precipitation Index* (SPI) to assess meteorological droughts using monthly precipitation time series.

The SPI is constructed through a probabilistic transformation process, where the probability density function of precipitation data is converted into a normal distribution. This transformation allows the SPI to express the deviation of monthly precipitation from the long-term mean (reference period) in terms of standard deviations. This standardization facilitates the comparison of drought severity across different regions, independent of local climatic and vegetative characteristics.

The first step in constructing the SPI is to establish the reference period, which is critical for fitting the normal distribution. McKee et al., 1993 recommended a minimum reference period of 30 years, which is sufficient to capture long-term climatic trends and reduce the influence of short-term variability. However, Laimighofer and Laaha, 2022 pointed out that a 30-year period might not adequately represent extreme precipitation events, potentially introducing biases. For a more robust analysis, a reference period of 50 years is often employed, as recommended in Guttman, 1999; Vidal, Martin, Franchistéguy, Habets, et al., 2010. In this study, a 50-year reference period starting in 1971 was selected. This starting date was chosen to ensure that all simulations had the same reference period, regardless of the date on which they began.

Once the reference period has been established, the subsequent step is to preprocess the monthly precipitation data. The monthly data are aggregated over specific timescales, resulting in the cumulative precipitation over the previous n months for each month, where n is typically one of the following values: 1, 3, 6, or 12 (McKee et al., 1993). These aggregation times facilitate the identification of various precipitation patterns (McKee et al., 1993; Zargar et al., 2011). McKee et al., 1993 posited that each aggregation period represents a typical timescale for precipitation to affect different water sources. Zargar et al., 2011 interpreted these aggregations as depicted in Table 2.1. Vidal, Martin, Franchistéguy, Habets, et al., 2010 recommended the use of several time scales to comprehensively characterize droughts, given that different socio-economic sectors would be impacted over different time scales. In this analysis, we have chosen to focus on short- and long-term precipitation patterns to identify droughts, using the one-month and twelve-month time scales.

Timescale	**Interpretation**
1 month	Short-term conditions affecting mainly crops during the growing season.
3 months	Short- and Medium-term conditions, representing a seasonal estimation of precipitation.
6 months	Medium-term trends in precipitation.
12 months	Long-term precipitation patterns, possibly affecting streamflow and water reservoir levels.

Table 2.1 – Interpretation of the aggregating timescale for SPI from Zargar et al., 2011.

This analysis aims to evaluate the deficiency of precipitation relative to the location and the climatology over a reference period. The relative deficit of precipitation in November shall be compared to that in July. Subsequently, as previously done by Vidal, Martin, Franchistéguy, Habets, et al., 2010; Vidal et al., 2012, the seasonal cycle is removed. This is achieved by calculating the mean precipitation for each month over the reference period and subtracting it from the data.

Once the data are preprocessed, they are fitted to a probability density function. McKee et al., 1993 originally proposed fitting a gamma distribution to the precipitation time series, as it was found to best represent the data. This choice has been validated by subsequent studies, such as Lloyd-Hughes and Saunders, 2002, who confirmed that the gamma distribution effectively represents precipitation patterns across much of Europe. However, the gamma distribution may not always be the most appropriate choice, depending on local climatic conditions and the spatial scale of the data. Studies by Laimighofer and Laaha, 2022; Lloyd-Hughes and Saunders, 2002; Pieper et al., 2020; Vidal, Martin, Franchistéguy, Habets, et al., 2010 have explored alternative parametric distributions, such as the Pearson Type III or the exponentiated Weibull distribution, which may offer better fits in certain contexts. Additionally, Naveau et al., 2016 proposed more complex parametric distributions designed to capture a broader range of precipitation behavior, including extreme events. Nonparametric approaches such as Gaussian kernel density estimation have also been used, as in Vidal, Martin, Franchistéguy, Habets, et al., 2010, providing flexibility in situations where parametric models are inadequate. After testing the normality of the standardized indices, the nonparametric distributions are used to represent the input variables in this analysis.

After fitting the probability density function to the data, the distribution is transformed into a normal distribution. The SPI value for a given month is then determined by finding the value at which the cumulative probability of the normal distribution matches the cumulative probability of the fitted precipitation distribution. This method ensures that the driest 5% of months, for instance, can be directly compared across different locations, regardless of local climatic conditions. The relation between the return period and the SPI's value is shown in 2.2.

SPI value	Probability to happen	Return period
< -0.84	20%	1:5
< -1.28	10%	1:10
< -1.64	5%	1:20
< -2.33	1%	1:100
< -3.09	0.1%	1:1000

Table 2.2 – Correspondance between the SPI value and the return period.

2.2.2. Extending Standardized Indices to Evapotranspiration and Soil Wetness

This process of standardization can be adapted to different variables, depending on the focus of the analysis.

Given the importance of evapotranspiration in drought dynamics, Vicente-Serrano et al., 2010 introduced the *Standardized Precipitation-Evapotranspiration Index* (SPEI). The SPEI uses net precipitation — calculated as precipitation minus PET — as its core variable, allowing for the assessment of drought conditions that consider both the supply (precipitation) and demand (atmospheric conditions) of water. This index is particularly useful for understanding how increasing temperatures and atmospheric changes, driven by climate change, can exacerbate drought conditions.

In this study, we aim to isolate the impact of PET on drought events, independent of precipitation effects. Thus, we introduce the *Standardized Potential Evapotranspiration Index* (SPETI), which applies the standardization process to the PET variable. This index provides insight into the atmospheric drivers of droughts, such as temperature and wind, and their contribution to humidity deficits.

Another relevant index for this analysis is the *Standardized Soil Wetness Index* (SSWI), as used in Vidal, Martin, Franchistéguy, Habets, et al., 2010. The SSWI is derived from the Soil Wetness Index (SWI), which was previously defined using the formula [2.1]. It measures anomalies in soil moisture content, directly reflecting agricultural drought conditions. By standardizing soil moisture data, the SSWI enables the comparison of soil moisture deficits across different regions and periods, offering a tool for assessing the severity and spatial extent of agricultural droughts.

The standardized indices used in this analysis are the Standardized Soil Wetness Index (SSWI), the Standardized Precipitation Index (SPI), and the Standardized Potential Evapotranspiration Index (SPETI). These standardized indices are built on two timescales: one-month and twelve-month aggregation time. To refer to an index built with one of these timescales, the timescale is written at the end of the index (e.g. SSWI1 and SSWI12). Each of these indices serves a specific purpose in our analysis:

- **Standardized Soil Wetness Index (SSWI)**: This index is used to identify and assess agricultural droughts by reflecting soil moisture anomalies. Drought detection, as developed below, is then performed on SSWI1 and SSWI12. Droughts detected in the first case are referred to as SSWI1 droughts, and those detected in the second case are referred to as SSWI12 droughts.

- **Standardized Precipitation Index (SPI)**: The SPI is used to study the impact of precipitation on agricultural droughts.

- **Standardized Potential Evapotranspiration Index (SPETI)**: The SPETI is used to study the impact of PET on agricultural droughts.

2.3. From Moisture Deficit to Drought Event

Now that we have seen how drought can be quantified, drought events must be detected and characterized in both space and time. As mentioned in the introduction, this analysis aims to study droughts as contiguous events across spatial and temporal scales.

Traditional methods of drought analysis are limited when dealing with spatio-temporal events, as discussed by Lloyd-Hughes, 2012. Techniques designed to extract recurrent spatial patterns assume temporal invariance, while those focused on temporal patterns are usually restricted to specific spatial domains. Furthermore, atmospheric space-time methods like extended empirical orthogonal functions often fail to reliably detect irregularly occurring features (Lloyd-Hughes, 2012). Therefore, a different approach is required to overcome these limitations in drought analysis. ## Initial Algorithm for Event Detection

The existing literature offers insights into techniques for analyzing drought events (Andreadis et al., 2005; Lloyd-Hughes, 2012; Tramblay et al., 2024; Vidal, Martin, Franchistéguy, Habets, et al., 2010; Vidal et al., 2012). These studies employ a common algorithm, with incremental improvements over time, culminating in the work by Lloyd-Hughes, 2012, which is specifically designed for spatiotemporal drought event detection.

The core of this algorithm involves creating clusters of contiguous points experiencing drought at each timestep and then linking these clusters across time if a sufficient number of points remain consistent between consecutive timesteps. Three key characteristics are critical for this algorithm:

1. **Threshold for Drought Intensity:** The threshold below which a drought is considered to occur at a given point.

2. **Minimum Cluster Size:** The minimum number of contiguous points required to form a cluster at each timestep, which helps define the spatial extent of a drought.

3. **Temporal Continuity:** The minimum number of identical points required between consecutive clusters over time to define a continuous drought event, which addresses the temporal aspect of drought displacement.

2.3.1. Connected Components in Three Dimensions

Updating the previous algorithm, Zscheischler et al., 2013 proposed an improved method that can be applied to analyzing various extreme events, not just droughts. This method, known as the *connected components* approach, has been applied in studies of heatwaves (Luo et al., 2024; Vogel et al., 2020) and gross primary production anomalies (Zscheischler et al., 2014).

The connected components algorithm detects spatio-temporal events by treating data as a collection of time series — one for each spatial location — where each value indicates whether an event is occurring. These data points are conceptualized as small cubes in a three-dimensional space, with two dimensions representing space and the third dimension representing time. The algorithm groups neighboring points (cubes) that are experiencing the event, where two cubes are considered neighbors if they share at least one vertex. Once these groups are identified, they can be filtered to retain only those events that meet a minimum size or duration criterion.

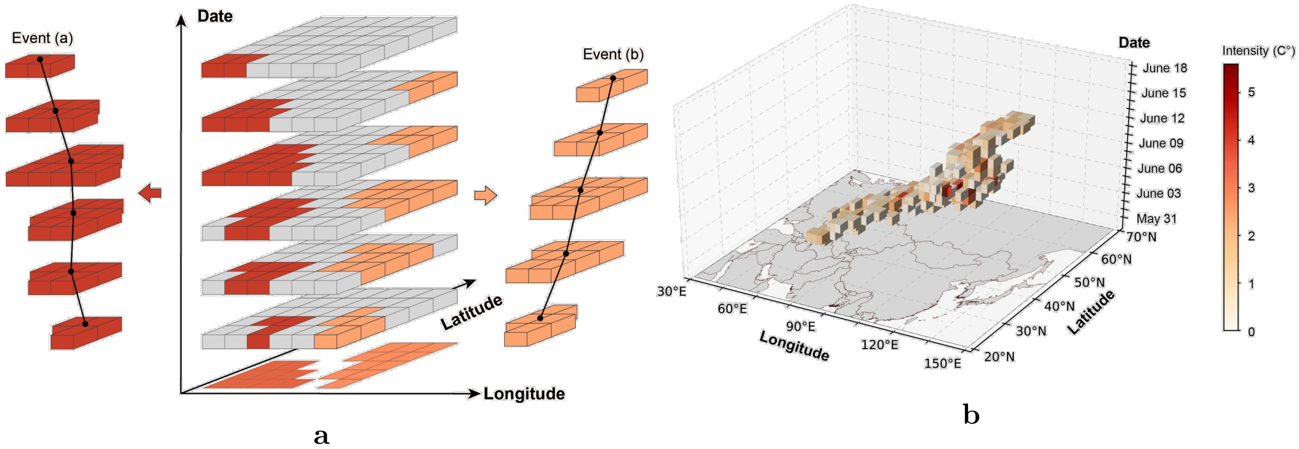

Figure 2.2 – Illustration of the Connected Components in 3 Dimensions (CC3D) algorithm used for heatwaves (Luo et al., 2024). The algorithm identifies spatiotemporally contiguous points facing an extreme event, with connectivity of 26 along the three dimensions: latitude × longitude × time. (a) shows two distinct events, represented by the red and orange colors, respectively, once CC3D algorithm has processed data in both spatial and temporal dimensions. (b) depicts a heatwave event over China identified by the CC3D algorithm between May 31 and June 17, 1997.

An illustration of the process can be found in Figure 2.2, copied from Luo et al., 2024. The illustration on the left panel depicts how the CC3D algorithm processes data in both spatial and temporal domains. Each colored cube is a dry gridpoint at a specific time step. Cubes are aggregated into an event if they are connected by either a face, an edge, or a vertex, otherwise known as connectivity 26. As illustrated in the figure, two events are identified: the red and the orange ones. The right panel depicts a heatwave that China experienced in 1997, which has been detected using the CC3D algorithm.

Zscheischler et al., 2013 underscored that the success of this method depends on how the data is pre-processed. The initial step is standardization, which ensures that data can be compared across space and time. Depending on the objective of the analysis, the seasonal cycle and the trend can be removed from the data. In this analysis, the impact of climate change is examined, and thus, the trend is retained. Otherwise, the standardization and removal of the seasonal cycle are conducted through the calculation of the SSWI, as detailed in section 2.2.

2.3.2. Data Preprocessing

This section outlines the three principal treatments that are applied once the SSWI has been computed. This study focuses on the analysis of the most extreme drought conditions. Subsequently, the five percent of droughts with the lowest SSWI values are identified, retaining only those points where the index is less than or equal to -1.64 (see Table 2.2).

To ensure temporal consistency and prevent the formation of spurious connections between drought events, a filter is applied to the time dimension. Points experiencing drought for just one month are kept only if their intensity is twice the threshold defining a drought (i.e., only if SSWI -3.28). This strict criterion guarantees that brief, isolated anomalies do not result in the erroneous identification of drought events. In the absence of such a filter, the Connected Components in 3 Dimensions (CC3D) algorithm may incorrectly establish links between distinct events due to the presence of occasional, isolated instances of drought.

A spatial filter is applied to ensure the contiguity of drought events. At each time step, only contiguous drought areas of 10 points or more are retained. This corresponds to a minimum area of 640 km^2, ensuring that only significant, spatially coherent drought events are considered. This criterion, similar to that used by Vidal, Martin, Franchistéguy, Habets, et al., 2010, excludes small, scattered drought patches that are less relevant for large-scale agricultural drought analysis.

In summary, the principal preprocessing steps employed in the analysis of the data are as follows:

1. **Selection of Severe Droughts (SSWI)**: The analysis focuses on the most severe 5% of drought conditions, as defined by the SPI -1.64 threshold.
2. **Time Consistency Filter (SSWI)**: Only those short-term drought points that exhibit a markedly elevated intensity (SSWI -3.28) are retained.
3. **Space Consistency Filter (SSWI)**: This ensures that drought events must cover a minimum of 640 kmš in a contiguous area to be considered spatially coherent.

The implementation of these preprocessing steps ensures that the subsequent analysis is centered on the most significant drought events, thereby establishing a robust foundation for the use of the CC3D algorithm. The application of the final two filters ensures that the algorithm proposed by Zscheischler et al., 2013 does not result in the grouping of multiple drought events into a single one. This discrepancy with the approach presented in this article can be attributed to the spatial scale of the data, with the aforementioned article using data at approximately 50 km x 50 km, whereas in our case, the data are on an 8 km x 8 km grid.

The thresholds employed in these preprocessing steps are heuristic as they have been set by examining the events resulting from the CC3D algorithm with regard to their shape, space, and time evolutions. As outlined in Wilhite, 2016, the thresholds used to define droughts are arbitrary as they are not directly correlated with specific socioeconomic impacts. These thresholds could be adapted according to the requirements of different stakeholders.

2.3.3. Postprocessing of Detected Events

Postprocessing steps are applied to refine the drought events detected by the CC3D algorithm. If the surface area of a detected event drops below 10% of the total studied area over any given time step, the event is split. This criterion prevents the over-aggregation of unrelated drought occurrences, ensuring that the identified events represent significant, contiguous drought periods rather than isolated or sporadic conditions. Then, events that persist for less than three months are discarded.

2.4. Analyzing Drought Events

Once the drought events have been identified and refined, they are characterized using several metrics to provide a detailed understanding of their properties. To assess the evolution of the extreme drought characteristics, the simulation period is divided into two phases: the past (up to 2025) and the future (from 2025 onwards). This temporal division facilitates a comparative analysis of drought characteristics and trends over time, allowing for an evaluation of how drought conditions may evolve with climate change.

2.4.1. Describing Drought Events

Once the drought events have been identified and refined, they are characterized using several metrics to provide a detailed understanding of their properties. Zargar et al., 2011 provided a comprehensive summary of commonly used metrics for characterizing drought. These metrics are designed to describe three main characteristics: duration, spatial extent, and intensity. To ensure the robustness of the characteristics assessment to extreme values, the median values are used rather than the average values. The metrics used in this analysis are listed in Table 2.3.

Characteristic	**Metric**	**Interpretation**
Spatial Extent	Median Surface	Median of the affected area at each time step, expressed in percentage of the total area. This metric quantifies the typical surface area affected by the drought over its duration.
Duration	Total Duration	Time from the start to the end of the drought event. This metric captures the overall length of the drought, indicating how long it persists.
Duration	Median Duration	Median of the times that each spatial point in the event spends under drought conditions. This metric provides insight into the consistency of drought conditions across the affected area.
Intensity	Cumulative Intensity	Sum of SSWI values over the event's duration in all the points affected by the drought. This metric aggregates the total drought intensity, combining both the extent (in space and time) and the severity of the drought.
Intensity	Median Intensity	Median SSWI value for the event. This metric reflects the overall severity of the drought, with lower values indicating more intense drought conditions.

Table 2.3 – Metrics used to describe drought events and their interpretations.

2.4.2. Attribution of Agricultural Droughts to Meteorological Factors

The main natural drivers of droughts are the lack of precipitation and the evapotranspiration. This analysis focuses on examining the roles of precipitation and PET in extreme agricultural droughts.

The method for attribution used in this analysis comes from Zscheischler et al., 2013. Zscheischler et al., 2014 applied it defining the events with gross primary production (GPP) anomalies, and exploring how different factors, such as temperature and precipitation, influenced these anomalies. The analysis of the lag time of these impacts — that is, the temporality of such events and the processes leading to droughts — allows us to understand how far in advance or how long after an event these factors have an effect.

Zscheischler et al., 2013 offers a framework for such analysis. Once events are defined in space and time, the median values of contributing factors within the event are calculated. These median values are then compared with median values of the same factors at different time lags, simulating the occurrence of the event i timesteps before or after. From this analysis, a time series of median values, one value per lag, is generated, and a p-value can be calculated to determine whether the contribution of a factor at a specific time lag is statistically extreme. For extremely low values, the p-value is defined as:

$$p_{low}^{value} = \frac{\#\left\{med_t < med_{t_0} | t \in N\right\}}{\#\left\{t \in N\right\}} \tag{2.2}$$

where # corresponds to the number of values in the set defined between the brackets. For high values, the p-value is calculated as:

$$p_{high}^{values} = 1 - p_{low}^{value} \tag{2.3}$$

This approach allows for an analysis of the timing and significance of factors contributing to drought events, providing a framework for understanding their dynamics.

The SPI is employed to assess the impact of precipitation on extreme agricultural droughts, whereas the SPETI permits the evaluation of the influence of PET. These indices facilitate the analysis of the impact of precipitation and PET, along with their variations, on extreme agricultural droughts. Additionally, the time lag between an extreme precipitation deficit or PET value and the onset of an extreme agricultural drought is examined. To determine the significance of observed changes in drought characteristics, statistical testing is conducted using p-values defined above (Equations 2.2 and 2.3). These tests are applied to droughts from both past and future periods.

3. Results

3.1. Models Validation

To validate the simulations in accurately reproducing severe droughts, as experienced in the past, we compare the outputs of the simulations with reanalysis data. Specifically, we consider all drought events that started during the reanalysis period, i.e., before 2021. The primary objective is to determine whether the characteristics of simulated droughts are consistent with those observed historically. To achieve a robust yet comprehensive comparison, we conduct the following analyses:

- **Drought Frequency**: To assess the number of droughts.
- **Median Drought Surface**: To evaluate the spatial extent of the droughts.
- **Median Drought Duration**: To analyze the duration of droughts.
- **Median Drought Intensity**: To compare the severity of extreme droughts.

3.1.1. Frequency

The first step is to evaluate whether the simulations accurately reproduce the frequency of droughts observed in historical reanalysis data. With the inherently chaotic nature of weather systems, a statistical approach is necessary to compare the number of droughts in the model outputs with those in the reanalysis.

The simulations and the reanalysis data cover different periods, not starting the same year, leading to different dataset length. To compare compare simulations and reanalysis, the number of detected droughts is standardized by the duration of each dataset, up to the final date of the reanalysis period. This normalization is referred to as drought density, defined as the number of droughts per month.

$$Drought\ density = \frac{Number\ of\ droughts}{Number\ of\ timesteps}$$

As a reference, 11 drought events were detected in the reanalysis data using SSWI1 as an indicator for agricultural droughts, and 9 events using SSWI12.

Initially, we calculate the ratio of drought densities between the simulations and the reanalysis. A ratio close to 1 indicates that a simulation effectively reproduces the frequency of droughts observed in the reanalysis. This ratio provides a clear and intuitive measure of model performance. As illustrated in the histogram, Figure 3.1, produced using this approach, the simulations tend to underestimate the number of drought events during the historical period. For both indices used to detect drought events, only one simulation produces slightly more droughts than the reanalysis. However, given the low number of events, a refined approach is necessary.

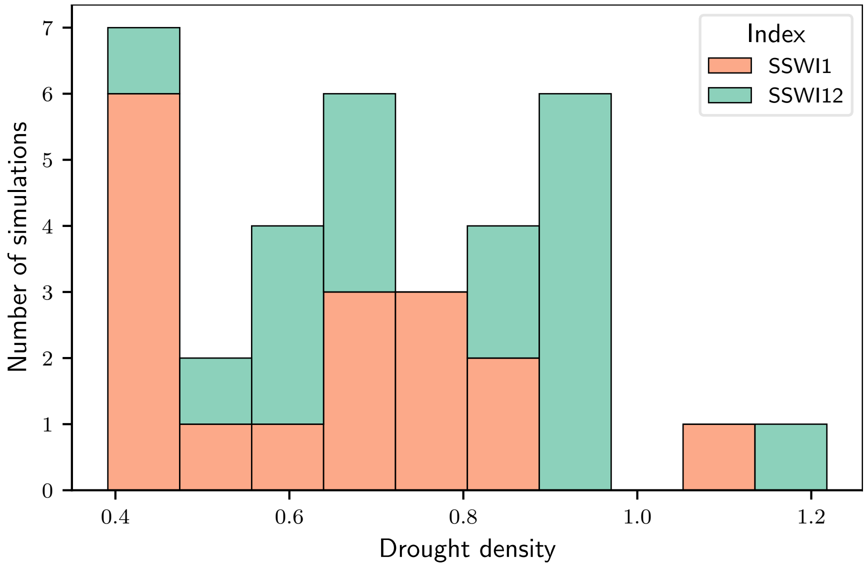

Figure 3.1 – Number of simulations per ratio of their drought densities (number of droughts per month) to the reanalysis drought density. If the ratio is less than 1, the simulation produces fewer droughts than the reanalysis, and vice versa.

To determine whether the differences between the simulations and the reanalysis are statistically significant, we employ a Z-test for proportions. This test assesses whether the proportion of droughts in each simulation differs significantly from that observed in the reanalysis, accounting for the size of each dataset. The Z-test is chosen for its simplicity and reliability, making it suitable for comparing proportions across different datasets. Notably, no simulation shows a statistically significant difference from the reanalysis according to this test.

For a more intuitive representation, we also calculate a confidence interval for the drought density observed in the reanalysis data. This interval, depicted as a black error bar in Figure 3.2, provides a range within which the true drought density is expected to fall with a certain level of confidence (99% in our case). This aims to account for the inherent chaos in the weather system. It is important to note that the higher the confidence level, the larger the confidence interval. The confidence interval has been computed using the Clopper–Pearson method (Clopper and Pearson, 1934). By comparing the drought densities from the simulations against this interval, we can evaluate whether the models' outputs are consistent with expectations based on the reanalysis.

In Figure 3.2, the drought density for each simulation is represented by a vertical bar. The four storylines highlighted throughout this report are color-coded according to their definitions, as detailed in the methodology section. The reanalysis's drought density is marked by a cross. As highlighted earlier, the vast majority of the simulations yield fewer drought events than the reanalysis. However, considering the chaotic nature of weather systems and the duration of each simulation, all these simulations produce plausible drought densities, as their values fall within the confidence interval.

3.1.2. Surface

Another characteristic to validate is the spatial extent of the droughts. To characterize this, we use the median of the affected area over time for each drought event, as explained in Section **??**. We begin by computing descriptive statistics to compare the simulations with the reanalysis

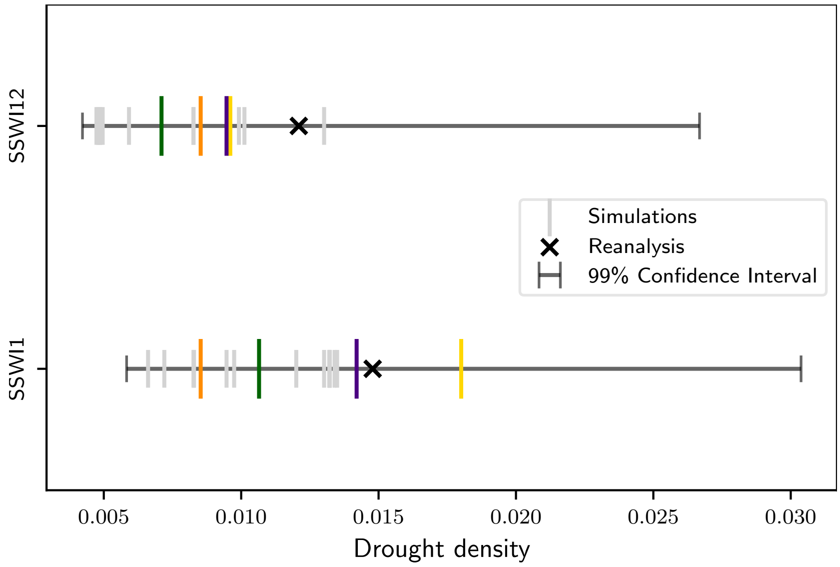

Figure 3.2 – Confidence interval for reanalysis drought density and simulation drought densities. The reanalysis drought density is marked by a cross and its 99% confidence interval by the black error bar.

data.

Next, the distributions of these surface areas are examined. As depicted in Figure 3.3, for SSWI1 droughts, the reanalysis (shown in black) falls within the envelope of all simulations. This indicates that some simulations reproduce wider droughts, while others yield narrower droughts. A closer inspection of the descriptive statistics reveals that the maximum spatial extent of the majority of simulations exceeds that observed in the reanalysis. Generally, simulations tend to produce droughts with a slightly larger surface area compared to the reanalysis. This discrepancy becomes more pronounced when considering SSWI12 droughts. In this case, all simulations exhibit broader droughts than those observed in the reanalysis. However, it is important to note that these observations are based on a relatively small number of events. While these insights are valuable, they cannot alone be used to invalidate the simulations for this type of study.

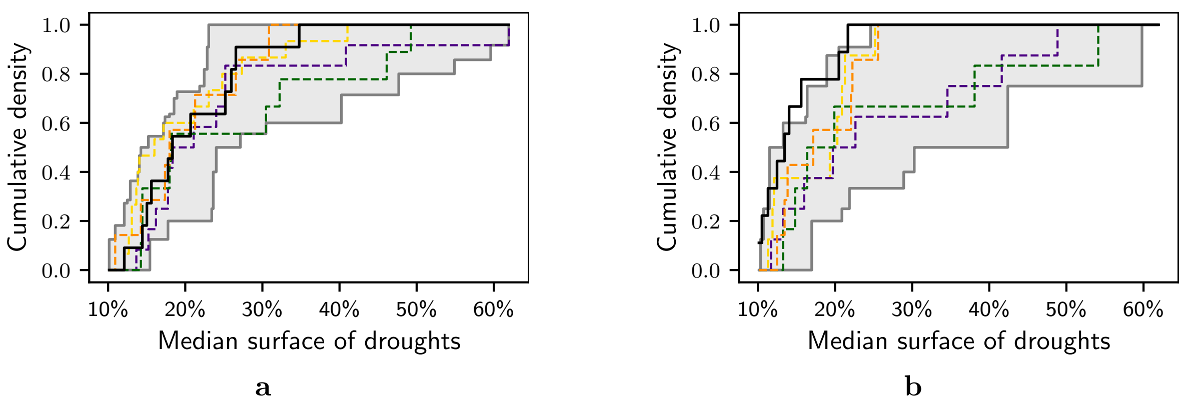

Figure 3.3 – Cumulative distribution of median drought surface area for (a) SSWI1 and (b) SSWI12 droughts. The reanalysis is shown in black.

To further refine the comparison, we employ a statistical test. The Mann-Whitney U test is selected for comparing drought characteristics between models outputs and reanalysis data due to its suitability for small sample sizes and its non-parametric nature. Unlike parametric tests, the Mann-Whitney U test does not assume normality and is robust against non-normal distributions. This test compares the ranks of the values between two independent groups, assessing whether the central tendencies of drought characteristics differ significantly, even with a limited number of events.

The results corroborate our earlier observations from the graphical analysis. For SSWI1 droughts, no simulation shows a significant difference from the reanalysis in terms of spatial extent at a 10% confidence level. However, when considering SSWI12 droughts, four simulations display a significant difference from the reanalysis at the same confidence level. Notably, two of these four simulations correspond to storylines highlighted throughout this report: the purple and the green storylines.

3.1.3. Duration

The same analysis is applied to drought duration. To characterize this, we use the median of the durations across the spatial extent for each event.

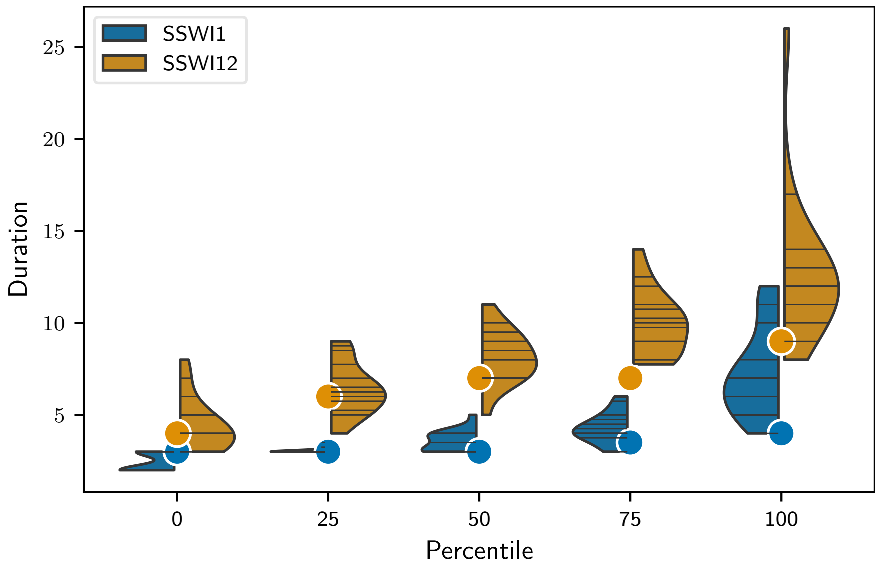

a

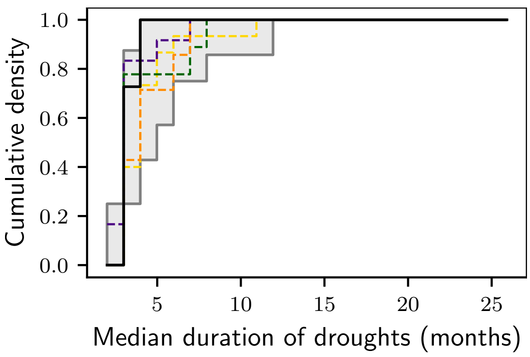

b

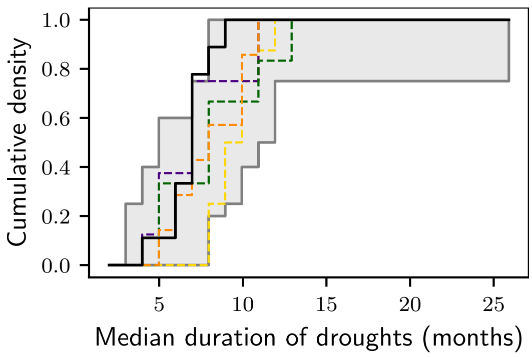

c

Figure 3.4 – Comparison of drought duration between simulations and reanalysis data. (a) Violin plot for the minimum, 25th percentile, median, 75th percentile, and maximum values of drought duration for each simulation. The reanalysis values are shown as circles. Cumulative distribution of median drought duration for (b) SSWI1 and (c) SSWI12 droughts. The reanalysis is shown in black.

We start with computing descriptive statistics and plotting the cumulative distributions. The layout of Figure 3.4 mirrors that used for the surface analysis. We observe that for both SSWI1 and SSWI12 indices, the simulations generally produce longer drought durations compared to the reanalysis. While the reanalysis data remains within the ensemble generated by the simulations, it is on the lower end of the spectrum. A closer examination of the descriptive statistics reveals that this discrepancy is most pronounced for the most extreme events, as illustrated in Figure 3.4a. In this figure, points represent percentiles of the reanalysis, while the colored areas indicate the percentiles of the simulations, with each simulation marked by a horizontal line within this area. For instance, for droughts detected using SSWI1, the discrepancies between the simulations and the reanalysis are minimal up to the third quartile; the third quartile for the reanalysis is 3.5 months, while the simulations range between 3 and 6 months (with only three simulations exceeding 5 months). The divergence becomes particularly marked for the longest droughts (maximum values).

As with the surface analysis, the Mann-Whitney U test is employed to identify any significant discrepancies between the simulations and the reanalysis. For drought duration, two simulations show significant differences from the reanalysis for SSWI1 droughts, and two for SSWI12 droughts. In both cases, the yellow storyline exhibits a deviation from the reanalysis. This deviation is also visible in the previous graphics, where the yellow storyline shows a distribution skewed toward longer droughts.

3.1.4. Intensity

The final characteristic to validate is the severity of the droughts. As done previously with other characteristics, we compute descriptive statistics and present cumulative distributions in Figure 3.5. The comparison reveals that the reanalysis and simulations produce drought events of similar intensities, which is coherent with the construction of standardized indices.

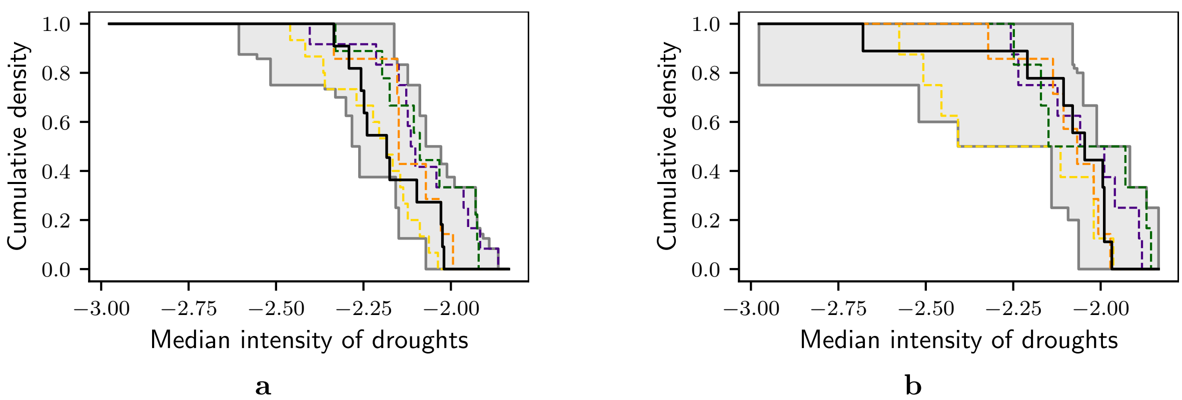

Figure 3.5 – Cumulative distribution of median drought intensity for (a) SSWI1 and (b) SSWI12 droughts. The reanalysis is shown in black.

This observation is confirmed by the Mann-Whitney U test, which indicates no significant differences between the reanalysis and the simulations in terms of drought intensity.

3.2. Evolution of Droughts

Having established that the ensemble of simulations sufficiently reproduces extreme droughts from the past, we now examine how these extreme droughts evolve over time within these simulations. The simulation periods are divided into two segments: before and after 2025, referred to as the past and future periods, respectively.

3.2.1. Statistical Changes

As a first step, we examine the overall changes in the characteristics of extreme droughts between the past and future periods. The number of extreme droughts per period is limited (around 10), which could introduce biases, even when using robust statistical methods.

The first question to address is how the frequency of extreme drought events changes over time. To do this, we calculate the drought densities, as defined in Section 3.1.1, for each simulation during the past and future periods. The ratio of drought density between the future and past periods for each simulation is then computed, represented in Figure 3.6. This ratio is straightforward to interpret: it represents how many times more frequent extreme droughts will be in the future compared to the past, with the ratio r indicating this change.

For both indices used in drought detection, the majority of simulations indicate an increase in drought frequency, with some showing up to a fourfold increase. The three storylines that show the most changes in precipitation and temperature simulate extreme drought events that are two to three times more frequent in the future than in the past. Of the 17 simulations, only four for SSWI1 droughts and six for SSWI12 droughts predict a reduction in the frequency of these events, with the yellow storyline being one of these projections.

As discussed in Section **??**, storylines are designed to represent the variability of climate change within the simulation ensemble using a limited number of simulations for easier interpretation. Here, we observe that the only storyline showing a decrease in drought density corresponds to a simulation with lower temperature increase and no precipitation change. In contrast, in the other three cases, where there are changes in temperature above +4.5°C, drought frequency increases in the future, suggesting that regardless of precipitation pattern changes, droughts are likely to become more frequent due to warming. For SSWI1 droughts, the highest frequency increase is seen in the simulation representing a drying climate, the orange storyline.

We then analyze the evolution of several drought characteristics: duration, surface, and intensity. Due to the limited number of events, for each index, we examine the evolution of the minimum, the 25th percentile (P25), the median, the 75th percentile (P75), and the maximum. We compute the ratio between the future and past values aforementioned to analyze the changes in the characteristics distributions. Furthermore, a Mann-Whitney U test is employed to identify central tendencies.

For the drought surface area, the Mann-Whitney U test identifies 4 (for SSWI1) and 3 (for SSWI12) simulations out of 17 where the median change is significant. The ratios of the 5 percentiles analyzed are shown in Figure 3.7a, with the four storylines highlighted by their specific colors. This figure shows that up to the median, simulations generally present a ratio close to 1, indicating no noticeable change in drought surface area. However, when focusing on the largest droughts, there is a wider dispersion of ratios among the simulations. For SSWI1 droughts, simulations generally do not show a significant change in surface area for the largest droughts, with a slight tendency towards smaller droughts. In contrast, the simulations for SSWI12 droughts demonstrate divergent trends for the most severe droughts. One simulation, the orange storyline, predicts a future maximum drought surface area that is approximately twice the size of the largest observed in the past, encompassing 58% of the territory. Another simulation, the green storyline, suggests that droughts may reach a maximum surface area that is only half the size of the largest observed in the past, or 40% of the territory. The most

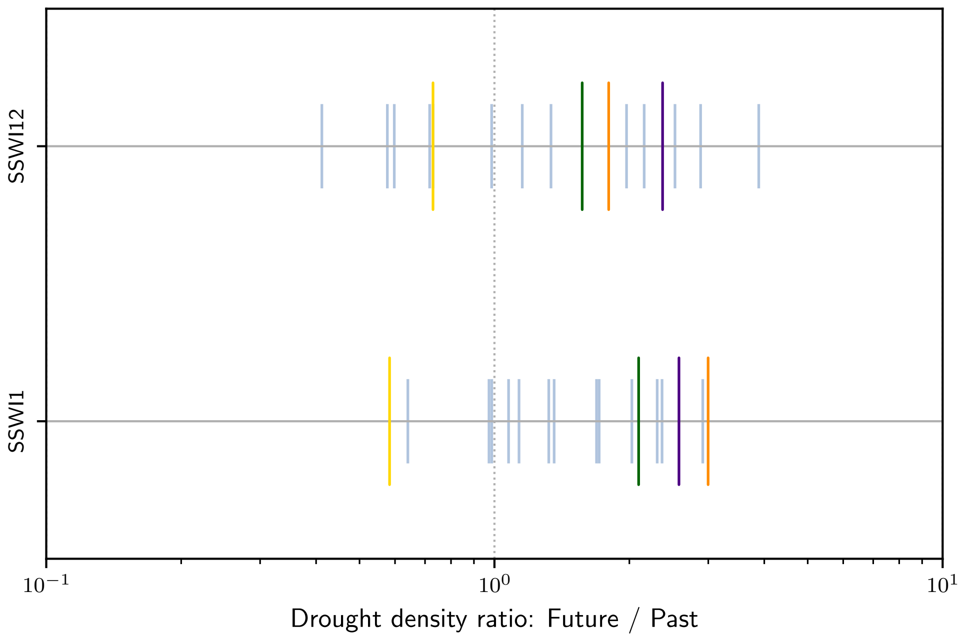

Figure 3.6 – Ratio of drought density (number of droughts per month) between the future and past periods for each simulation. Each simulation is marked with a vertical line and storylines are highlighted with colored lines. The x-axis is displayed on a logarithmic scale for clarity, as a ratio of 0.5 implies that extreme droughts will be half as frequent in the future.

significant changes in drought surface area occur in the most extreme cases in both instances.

When analyzing the evolution of drought duration, similar outcomes are observed from the Mann-Whitney U test: only two (for SSWI1) and five (for SSWI12) simulations out of 17 show a significant change at a 20% confidence level for the median drought duration between the past and future. However, a closer look at the distribution of drought durations reveals that the most substantial changes occur for the longest droughts. The majority of simulations predict longer droughts in the future up to nine times for the orange storyline that reaches a drought with a median duration of 109 months, as illustrated in Figure 3.7b for SSWI1 and SSWI12 droughts. Three simulations, including the yellow storyline, predict shorter maximum SSWI1 drought.

Finally, the intensity of past and future droughts is examined. Unlike surface area and duration, 9 (for SSWI1) and 8 (for SSWI12) simulations out of 17 exhibit a significant change in drought intensity according to the Mann-Whitney U test. Figure 3.7c presents these results, similar to the graphics used for duration and surface characteristics. In contrast to the other characteristics, drought intensity is represented as a negative value, meaning that the most severe droughts have the lowest values. The ratios are generally close to 1, indicating small changes; however, 9 (for SSWI1) and 10 (for SSWI12) simulations agree on an intensification of droughts for all quantiles (ratio greater than 1). As with the other characteristics, this ratio is more pronounced for the most intense droughts.

This analysis indicates that the frequency and intensity of droughts are likely to increase with climate change. For duration and surface area, the changes are not statistically significant with the small sample sizes representing extreme droughts in each period within the simulations. However, for all three characteristics, the more extreme the drought, the more significant the change. We will now explore the changes in the most extreme droughts observed in the past

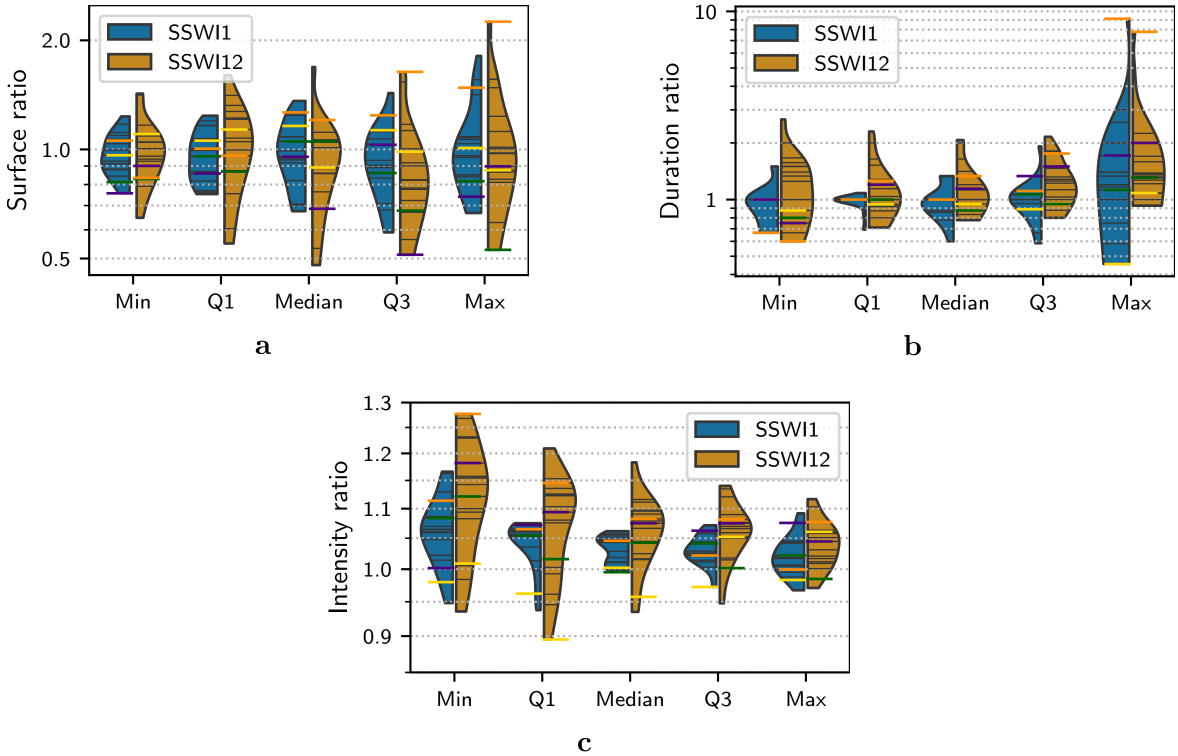

Figure 3.7 – Ratio of drought characteristics, (a) for the surface area, (b) for the duration, and (c) for the intensity, between the future and past periods for each simulation. The contour represents the distribution of these ratios. Storylines are highlighted with colored arrows.

and future across all simulations.

3.2.2. Focus on the Most Extreme Events in the Past and the Future

In this subsection, we focus on the changes observed in the most extreme droughts. We define the most extreme droughts based on their cumulative intensity, which corresponds to the minimum value since intensity is negative. By definition, cumulative intensity integrates the surface area, duration, and intensity of the drought, providing a comprehensive measure of its severity.

For each simulation, the most extreme droughts in both the past and future periods are identified. These droughts are plotted on a timeline below (Figure 3.8), for both SSWI1 and SSWI12 droughts.

One of the first observations is that, in most simulations, the most extreme droughts tend to start around the same dates for both SSWI1 and SSWI12 droughts. Additionally, in the future period, the most severe droughts are concentrated in the latter half of the 21st century, though they are not exclusively at the very end, as seen in the yellow storyline.

Characteristics of Extreme Droughts

To better understand the nature of these droughts, Figure 3.9 illustrates the distribution of their characteristics—surface area, duration, and intensity—for both the past and future periods across all simulations. These figures reveal the relative importance of each characteristic in defining the most extreme droughts.

Firstly, the surface area of these droughts appears not to be a decisive factor, varying signifi-

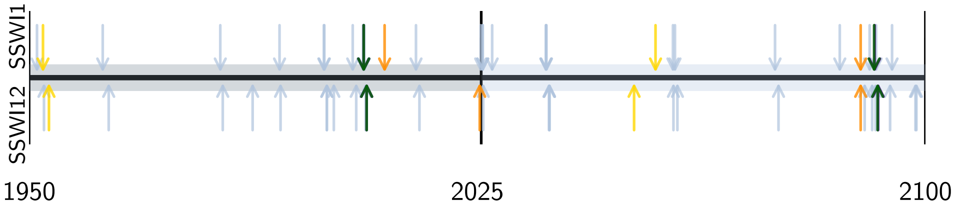

Figure 3.8 – Timeline of the most extreme SSWI1 (above the timeline) and SSWI12 (under the timeline) droughts in the past and future periods for each simulation. The most extreme droughts are defined based on their cumulative intensity. Arrows indicate the start date of the most extreme droughts. Green and purple storylines are overlaid.

cantly from 10% to 70% depending on the simulation. The distribution of surface area does not change markedly between past and future droughts, with some simulations predicting larger future droughts while others predict smaller ones, effectively balancing each other out.

In contrast, the duration of these droughts increases for all simulations except 6 for SSWI1 and 3 for SSWI12 between past and future periods. One simulation, the orange storyline, projects a 15-year drought detected with both SSWI1 and SSWI12 indices towards the end of the 21st century. Apart from the yellow storyline, the other three storylines exhibit a significant increase in the duration of the most extreme droughts.

Similarly, the intensity of these droughts increases in all the simulations except 6 for SSWI1 and 3 for SSWI12. There is a shift in the distribution towards more extreme values, with median intensity reaching up to -3.4 — a level indicating an exceptionally severe drought, with a probability of occurrence of just 0.03% in the reference period.

Detailed Analysis of Storylines

Focusing on the four storylines, we analyze the evolution of their worst droughts using the ratio of four metrics between the most extreme future and past droughts. The first metric is the total cumulative intensity, which determines the severity of the worst droughts. This metric helps us understand how much more severe the selected drought is in the future compared to the past. This overall change is then decomposed into the evolution of three characteristics — median duration, surface area, and intensity — to identify which aspects of these extreme droughts evolve the most. The changes observed in SSWI1 and SSWI12 droughts are similar as shown in Figure 3.10, so only the SSWI1 droughts are detailed here.

The three storylines that exhibit the most significant changes in temperature and precipitation due to anthropogenic greenhouse gas emissions — the orange, purple, and green storylines — predict a worsening of the most extreme droughts. In these future scenarios, extreme droughts are projected to be twice (green and purple storylines) to twenty times (orange storyline) more severe than those in the past. These storylines forecast different changes in precipitation but share a common prediction of strong warming, with average temperature increases of 4.6°C to 5°C over mainland France. The orange storyline, in particular, simulates a drier and warmer future, which sets the stage for severe droughts, as reflected in the projections.

For the orange storyline, the future's most extreme drought is slightly more intense, twice as wide, and ten times longer than the most extreme drought in the past. This highlights that

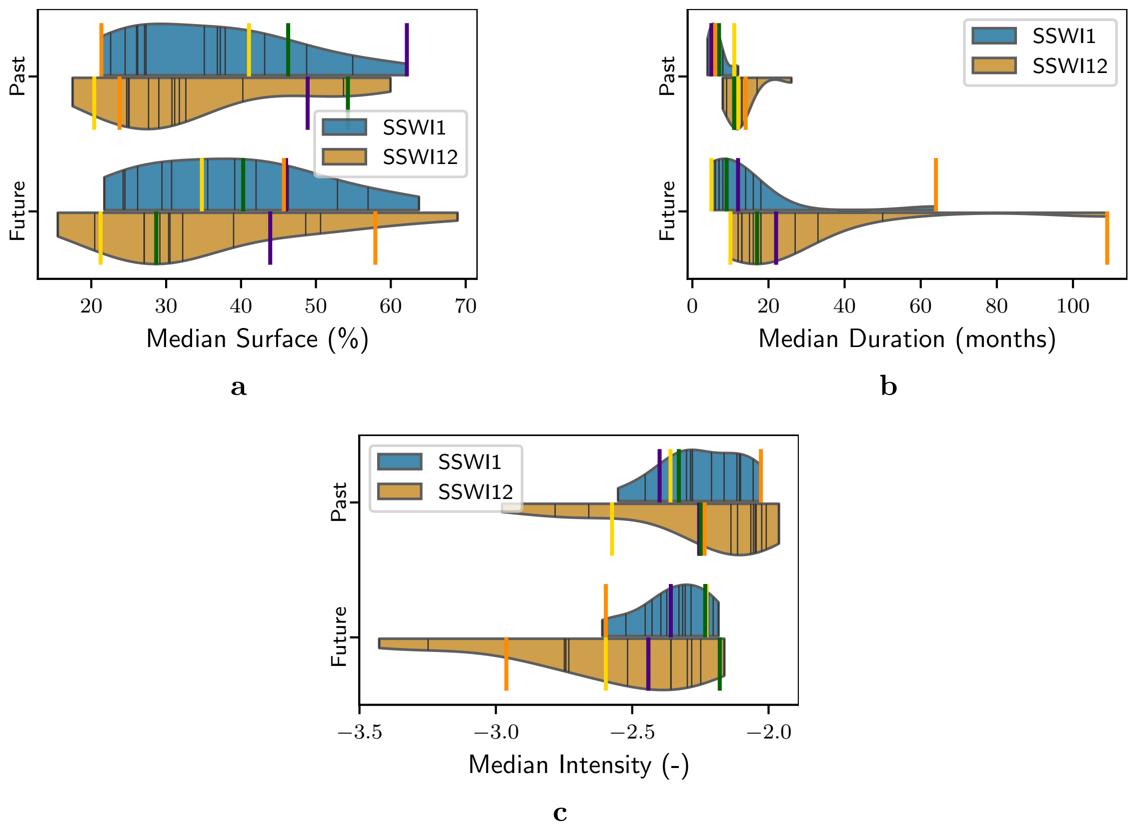

Figure 3.9 – Distribution of the characteristics of the most extreme droughts in the past and future periods for each simulation, (a) for the surface area, (b) for the duration, and (c) for the intensity. The most extreme droughts are defined based on their cumulative intensity.

duration is the key characteristic driving the worsening of future droughts. While the affected area tends to decrease slightly and median intensity remains relatively constant, the purple and green storylines also predict much longer extreme droughts than those experienced in the past.

Conversely, the yellow storyline presents an alternative scenario. This storyline shows less changes compared to the ensemble, leading to a lower level of warming (+3.7°C on average over mainland France) and a slightly wetter climate with a 6% increase in annual precipitation. This scenario results in a future extreme drought that is 2.5 times less severe than the worst drought experienced in the past. In this scenario, the future's most extreme drought is shorter, lasting only one year compared to the three years of the past extreme drought, with no significant changes in the other two characteristics.

3.3. Attribution of Agricultural Droughts to Meteorological Factor

From a meteorological point of view, agricultural droughts are driven by two main factors: precipitation and potential evapotranspiration. For a better understanding of these droughts' evolution, we explore the impact precipitation and PET on the evolution of extreme droughts. The methodology described in Section 2.4.2 is used to calculate p-values, with a 10% confidence level to determine if a factor is considered as extreme.

There may be a delay between an extreme precipitation deficit or a high PET and the onset

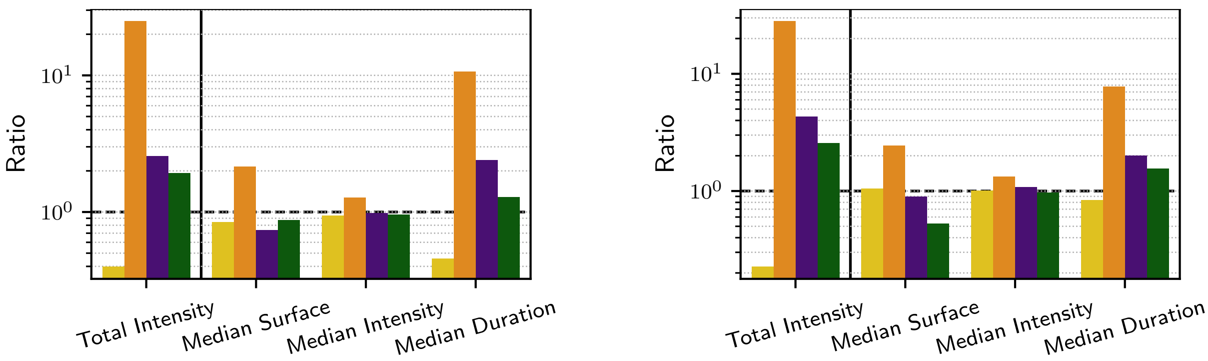

a b

Figure 3.10 – Ratio of the most extreme drought characteristics between the future and past periods for each storyline for (a) SSWI1 and (b) SSWI12 droughts. The most extreme droughts are defined based on their cumulative intensity.

of an agricultural drought. To account for this, we test lags ranging from 0 to 12 months before the drought event, resulting in 12 different p-values. Once computed, the number of drought events with significant levels of each factor is assessed and normalized by the total number of extreme events detected in each simulation and period.

3.3.1. Precipitation's Role in Extreme Droughts

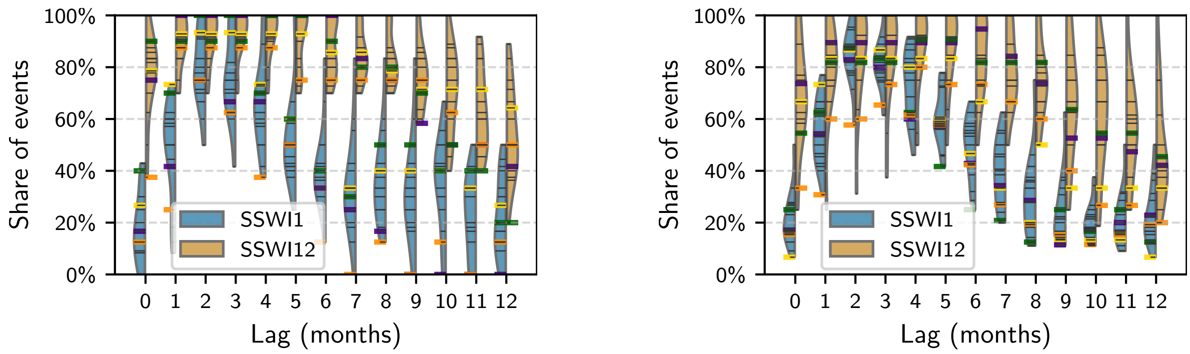

a b

Figure 3.11 – Proportion of extreme agricultural droughts associated with significant precipitation deficits for different lags and indices used for drought detection. The vertical lines represent each simulation. (a) Past period. (b) Future period.

Figures 3.11 depict the proportion of extreme agricultural droughts (y-axis) associated with significant precipitation deficiencies across all simulations (each marked by a vertical line). These distributions are shown for lags from 0 to 12 months and for SSWI1 and SSWI12 droughts.

A notable finding is that the delay between precipitation deficit and soil drought remains consistent between past and future periods. 50% to 100% of SSWI1 droughts occur 2 to 3 months after an extreme precipitation deficit, depending on the simulation. For SSWI12 droughts, the lag is longer, with extreme droughts often following a 1 to 9-month period of low precipitation. This discrepancy is likely due to the 12-month aggregation window for SSWI12, which captures the annual precipitation cycle's impact on soil wetness. It suggests that for SSWI12, a sustained 9-month period of precipitation deficit often precedes extreme droughts.

This period tends to shorten for future droughts, suggesting that other factors, such as PET, might be playing a more significant role in driving droughts under future climate conditions.

The overall contribution of precipitation to soil drought remains consistent between past and future periods, although slightly more droughts are correlated with extreme precipitation deficits in the future for SSWI1. For SSWI12, the change is reversed, with slightly fewer future droughts associated with precipitation deficits. This stability implies that precipitation will continue to be a major contributor to agricultural droughts, with most extreme droughts following a period of significantly low precipitation.

When examining the four storylines, the green, yellow, and purple ones exhibit a strong correlation between soil droughts and extreme precipitation deficits, with most droughts following such deficits. However, the orange storyline shows a significant reduction in this correlation for future droughts, likely due to its simulation of a drier and warmer future climate. This suggests that in such a scenario, other factors could be more influential in triggering droughts.

Last, the shape of the curves suggests that precipitation deficiencies accumulate over several months—at least 6 months for SSWI1 and up to 12 months for SSWI12—before resulting in an extreme drought.

3.3.2. PET's Role in Extreme Droughts

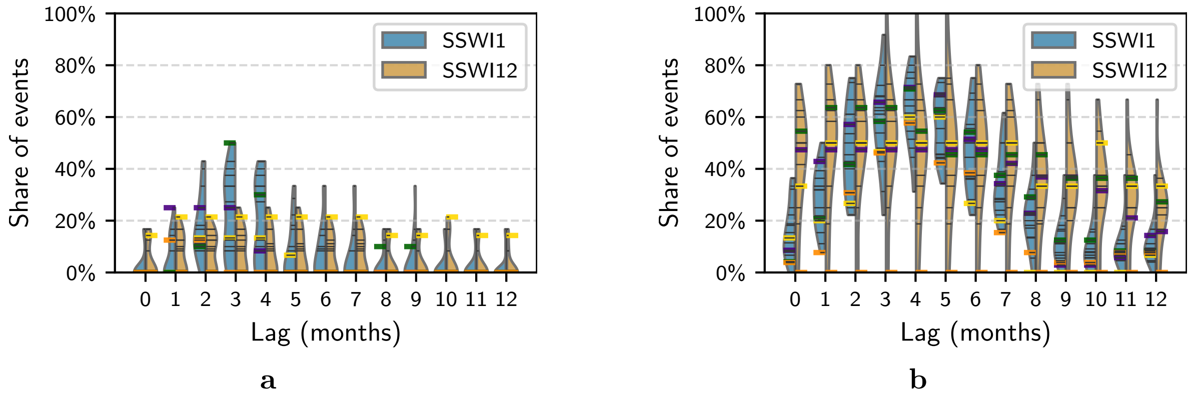

Figure 3.12 – Proportion of extreme agricultural droughts associated with significant PET values for different lags and indices used for drought detection. The vertical lines represent each simulation. (a) Past period. (b) Future period.

Similar to precipitation, Figure 3.12 illustrate the contribution of PET to past and future extreme agricultural droughts.

PET becomes significantly more extreme in future droughts. The increase of temperatures in all the simulations lead to higher PET values in the future. However, the variability of PET means that extreme droughts may not necessarily follow extreme PET values. Furthermore, not all simulations have the same increase in PET. Despite this variability, nearly all simulations show that future droughts are increasingly influenced by PET, contributing to the changes observed in drought characteristics.

The interval between the occurrence of high PET and the onset of drought varies between three and five months, as illustrated in Figure 3.12. This delay highlights the time frame within which the effects of elevated PET are manifested as soil moisture deficits.

It should be noted that an exception is made for SSWI12 droughts in the orange storyline. In this scenario, the variability of PET is low in comparison to its trend, indicating that PET values are generally higher in the future. The values reached by PET prior to a drought are then surpassed by those during and after this drought. This lower variability could explain why PET's role in droughts is less pronounced in this specific storyline with the method used.

4. Discussion and Conclusion

The validation process has demonstrated that the simulations are capable of replicating extreme droughts that are comparable to those observed in the past, with minor deviations. Firstly, the frequency of extreme droughts appears to be lower in almost all simulations in comparison to the reanalysis data for this period. Moreover, the simulations tend to generate extreme droughts that are larger and longer than those documented in the reanalysis, but these differencies are not statistically significant. It is, however, noteworthy that three of the four storylines exhibit one characteristic that differs significantly from that observed in the reanalysis. In particular, the purple and green storylines result in significantly larger extreme droughts than the reanalysis, but solely for SSWI12 droughts. The yellow storyline demonstrates a proclivity for longer droughts than the reanalysis, particularly for SSWI1 and SSWI12 droughts.

The analysis of extreme drought evolution has revealed that identifying a significant change in extreme drought characteristics is challenging due to the limited number of events that have been detected. The frequency and intensity of these droughts will likely increase in response to continued greenhouse gas emissions. In examining the most extreme droughts, the characteristic that demonstrates the most significant change is the duration. In both analyses, the storyline with the lowest projected warming over metropolitan France represents the opposite trend, whereby the characteristics of past extreme droughts are maintained or even reduced.

A notable lag of two to three months has been observed between the occurrence of precipitation deficits and the onset of soil moisture deficits. Long-term droughts are also affected by extended periods of low annual precipitation. While climate change does not significantly alter precipitation's contribution to agricultural droughts, it does increase the contribution of potential evapotranspiration (PET). PET levels rise in all simulations, though the rate of increase varies. This suggests that future agricultural droughts will be more heavily influenced by PET, with the evolution of drought characteristics, as detailed in the previous sections, likely driven by these increasing PET levels.

Inherent uncertainties and limitations are present in the data and methods that were employed for this analysis. As outlined in Section 2.1.2, each stage of the modeling process is associated with uncertainties (Evin et al., 2024a). The use of an ensemble of simulations allows for the assessment of these uncertainties. The various potential futures associated with the emission scenarios result in disparate evolutions for droughts in France. Tramblay et al., 2024 showed that the RCP 8.5 scenario exhibited the most significant alterations in drought characteristics.

Global climate models (GCMs) and regional climate models (RCMs) do not all model the same processes, which leads to different responses to emission scenarios. The EURO-CORDEX ensemble has been assessed in Vautard et al., 2021, and the authors concluded that the main variables were represented in a manner close to observations. However, they also detected several systematic biases in the GCM-RCM couples. On average, the simulations were found to be colder, wetter, and windier than observations. Some presented strong biases on one of these characteristics.

Bias correction methods are statistical techniques employed to align model outputs with observed data. Some researchers have expressed reservations about their use. These methods are unable to correct significant errors inherent to the model, thus the limits of their efficacy must be known for well-informed results (Maraun et al., 2017). In the EXPLORE2 project, three bias correction methods have been tested, with the results indicating a high degree of similarity in the outputs produced by the various methods (Robin et al., 2023). Evin et al., 2024a demonstrated that the impact of bias correction methods on the simulations within the EXPLORE2 ensemble is comparatively minimal in comparison to that of the GCMs, RCMs, and LSMs.

In É. Sauquet et al., 2023, the LSMs employed in the EXPLORE2 project were evaluated, and their uncertainties were outlined in Evin et al., 2024a. É. Sauquet et al., 2023 conducted a validation of all the LSMs using historical data. Evin et al., 2024a observed that ORCHIDEE projected a greater number of changes in comparison to the other models. However, Evin et al., 2024a also elucidated that CO_2 exerts an influence on vegetation by limiting transpiration and stimulating growth. This impact is solely incorporated into the ORCHIDEE model, despite the inherent uncertainty in its representation (Evin et al., 2024a). They demonstrated that the elevated flows simulated with ORCHIDEE can be attributed to this effect. The potential link between extreme drought and CO_2 levels could also be investigated in light of this impact on vegetation.

The ORCHIDEE simulations used in this analysis do not incorporate changes in human behavior, including those related to water management, such as irrigation and land-use changes. These two behaviors exert an influence on the availability of water resources, and the feedback loops must be subjected to further investigation (Van Loon, Gleeson, et al., 2016; Van Loon, Stahl, et al., 2016).

Furthermore, limitations are imposed by the definition and detection of droughts employed in this analysis. As it has been stated on numerous occasions within this document, there is no universal definition of a drought, and this definition impacts the analysis. Moreover, the thresholds employed to identify episodes of drought are heuristic and thus require adaptation and discussion in accordance with the specific circumstances. A study on the sensitivity of the results to the choice of thresholds could be conducted to assess the robustness of the results.

The focus on the most extreme droughts resulted in median projections for the future that were less pronounced than those observed in Vidal et al., 2012. It would be instructive to focus on specific events, which would facilitate dialogue with stakeholders. As outlined in Chapter 1, an event-based storyline approach can facilitate a more profound comprehension of these phenomena (Shepherd, 2016, 2019). Furthermore, the construction of such storylines allows for the examination of anthropogenic influences, including the modeling of irrigation and land use change. This is already a feature of the ORCHIDEE model (de Rosnay et al., 2003; d'Orgeval and Polcher, 2008; Guimberteau et al., 2012; Piao et al., 2007).

The analysis could be extended to encompass hydrological droughts. The use of the *Standardized Runoff Index* (SRI) could be employed to assess the impact of climate change on hydrological droughts. This index is based on the same principles as the SSWI, but it is calculated using runoff data.

Bibliography

AghaKouchak, A., Mirchi, A., Madani, K., Di Baldassarre, G., Nazemi, A., Alborzi, A., Anjileli, H., Azarderakhsh, M., Chiang, F., Hassanzadeh, E., Huning, L. S., Mallakpour, I., Martinez, A., Mazdiyasni, O., Moftakhari, H., Norouzi, H., Sadegh, M., Sadeqi, D., Van Loon, A. F., & Wanders, N. (2021). Anthropogenic drought: Definition, challenges, and opportunities. *Reviews of Geophysics*, *59*(2), e2019RG000683. https://doi.org/10.1029/2019RG000683

Aldunce, P., Araya, D., Sapiain, R., Ramos, I., Lillo, G., Urquiza, A., & Garreaud, R. (2017). Local Perception of Drought Impacts in a Changing Climate: The Mega-Drought in Central Chile. *Sustainability*, *9*(11), 2053. https://doi.org/10.3390/su9112053

Allen, R. G. (Ed.). (2000). *Crop evapotranspiration: Guidelines for computing crop water requirements* (repr). Food and Agriculture Organization of the United Nations.

Andreadis, K. M., Clark, E. A., Wood, A. W., Hamlet, A. F., & Lettenmaier, D. P. (2005). Twentieth-Century Drought in the Conterminous United States. *Journal of Hydrometeorology*, *6*(6), 985–1001. https://doi.org/10.1175/JHM450.1

Antoni, V., & Joassard, I. (2024, January). *Chiffres clés des risques naturels - Edition 2023*. le service des données et études statistiques (SDES. Retrieved July 17, 2024, from https://www.statistiques.developpement-durable.gouv.fr/edition-numerique/chiffres-cles-risques-naturels-2023/livre

Barbero, R., Curt, T., Ganteaume, A., Maillé, E., Jappiot, M., & Bellet, A. (2019). Simulating the effects of weather and climate on large wildfires in France. *Natural Hazards and Earth System Sciences*, *19*(2), 441–454. https://doi.org/10.5194/nhess-19-441-2019

Boé, J., & Habets, F. (2014). Multi-decadal river flow variations in France. *Hydrology and Earth System Sciences*, *18*(2), 691–708. https://doi.org/10.5194/hess-18-691-2014

Clarke, B., Otto, F., Stuart-Smith, R., & Harrington, L. (2022). Extreme weather impacts of climate change: An attribution perspective. *Environmental Research: Climate*, *1*(1), 012001. https://doi.org/10.1088/2752-5295/ac6e7d

Clopper, C. J., & Pearson, E. S. (1934). THE USE OF CONFIDENCE OR FIDUCIAL LIMITS ILLUSTRATED IN THE CASE OF THE BINOMIAL. *Biometrika*, *26*(4), 404–413. https://doi.org/10.1093/biomet/26.4.404

Cook, B. I., Mankin, J. S., & Anchukaitis, K. J. (2018). Climate Change and Drought: From Past to Future. *Current Climate Change Reports*, *4*(2), 164–179. https://doi.org/10.1007/s40641-018-0093-2

de Rosnay, P., Polcher, J., Laval, K., & Sabre, M. (2003). Integrated parameterization of irrigation in the land surface model ORCHIDEE. Validation over Indian Peninsula. *Geophysical Research Letters*, *30*(19). https://doi.org/10.1029/2003GL018024

Dirmeyer, P. A., Dolman, A. J., & Sato, N. (1999). The Pilot Phase of the Global Soil Wetness Project. *Bulletin of the American Meteorological Society*, *80*(5), 851–878. https://doi.org/10.1175/1520-0477(1999)080<0851:TPPOTG>2.0.CO;2

d'Orgeval, T., & Polcher, J. (2008). Impacts of precipitation events and land-use changes on West African river discharges during the years 1951–2000. *Climate Dynamics*, *31*(2), 249–262. https://doi.org/10.1007/s00382-007-0350-x

Evin, G., Hingray, B., Reverdy, A., Ducharne, A., & Sauquet, E. (2024a, June 7). *Ensemble de projections explore2 : Changements moyens et incertitudes associées*. EXPLORE2.

Evin, G., Hingray, B., Reverdy, A., Ducharne, A., & Sauquet, E. (2024b, June 7). *Matériel supplémentaire de "ensemble de projections explore2 : Changements moyens et incertitudes associées"*. EXPLORE2.

Garreaud, R. D., Alvarez-Garreton, C., Barichivich, J., Boisier, J. P., Christie, D., Galleguillos, M., LeQuesne, C., McPhee, J., & Zambrano-Bigiarini, M. (2017). The 2010–2015 megadrought in central Chile: Impacts on regional hydroclimate and vegetation. *Hydrology and Earth System Sciences*, *21*(12), 6307–6327. https://doi.org/10.5194/hess-21-6307-2017

Garreaud, R. D., Boisier, J. P., Rondanelli, R., Montecinos, A., Sepúlveda, H. H., & Veloso-Aguila, D. (2020). The Central Chile Mega Drought (2010–2018): A climate dynamics perspective. *International Journal of Climatology*, *40*(1), 421–439. https://doi.org/10.1002/joc.6219

Giorgi, F., & Jr, W. J. G. (2015). Regional Dynamical Downscaling and the CORDEX Initiative. *Annual Review of Environment and Resources*, *40*, 467–490. https://doi.org/10.1146/annurev-environ-102014-021217

Giuntoli, I., Renard, B., Vidal, J. .-., & Bard, A. (2013). Low flows in France and their relationship to large-scale climate indices. *Journal of Hydrology*, *482*, 105–118. https://doi.org/10.1016/j.jhydrol.2012.12.038

Gourdier, S., & Plat, E. (2018). Impact du changement climatique sur la sinistralité due au retrait-gonflement des argiles. Retrieved August 13, 2024, from https://brgm.hal.science/hal-01768395

Guimberteau, M., Laval, K., Perrier, A., & Polcher, J. (2012). Global effect of irrigation and its impact on the onset of the Indian summer monsoon. *Climate Dynamics*, *39*(6), 1329–1348. https://doi.org/10.1007/s00382-011-1252-5

Guttman, N. B. (1999). Accepting the Standardized Precipitation Index: A Calculation Algorithm. *JAWRA Journal of the American Water Resources Association*, *35*(2), 311–322. https://doi.org/10.1111/j.1752-1688.1999.tb03592.x

Habets, F., Boone, A., Champeaux, J. L., Etchevers, P., Franchistéguy, L., Leblois, E., Ledoux, E., Le Moigne, P., Martin, E., Morel, S., Noilhan, J., Quintana Seguí, P., Rousset-Regimbeau, F., & Viennot, P. (2008). The SAFRAN-ISBA-MODCOU hydrometeorological model applied over France. *Journal of Geophysical Research: Atmospheres*, *113*(D6). https://doi.org/10.1029/2007JD008548

Hargreaves, G. H., & Samani, Z. A. (1985). Reference Crop Evapotranspiration from Temperature. *Applied Engineering in Agriculture*, *1*(2), 96–99. https://doi.org/10.13031/2013.26773

IPCC. (2023a, July 6). *Climate Change 2021 – The Physical Science Basis: Working Group I Contribution to the Sixth Assessment Report of the Intergovernmental Panel on Climate Change* (1st ed.). Cambridge University Press. https://doi.org/10.1017/9781009157896

IPCC. (2023b, June 22). *Climate Change 2022 – Impacts, Adaptation and Vulnerability: Working Group II Contribution to the Sixth Assessment Report of the Intergovernmental Panel on Climate Change* (1st ed.). Cambridge University Press. https://doi.org/10.1017/9781009325844

Jacob, D., Petersen, J., Eggert, B., Alias, A., Christensen, O. B., Bouwer, L. M., Braun, A., Colette, A., Déqué, M., Georgievski, G., Georgopoulou, E., Gobiet, A., Menut, L., Nikulin, G., Haensler, A., Hempelmann, N., Jones, C., Keuler, K., Kovats, S., . . . Yiou, P. (2014). EURO-CORDEX: New high-resolution climate change projections for European impact research. *Regional Environmental Change*, *14*(2), 563–578. https://doi.org/10.1007/s10113-013-0499-2

Krinner, G., Viovy, N., de Noblet-Ducoudré, N., Ogée, J., Polcher, J., Friedlingstein, P., Ciais, P., Sitch, S., & Prentice, I. C. (2005). A dynamic global vegetation model for studies of the coupled atmosphere-biosphere system. *Global Biogeochemical Cycles*, *19*(1). https://doi.org/10.1029/2003GB002199

Laimighofer, J., & Laaha, G. (2022). How standard are standardized drought indices? Uncertainty components for the SPI & SPEI case. *Journal of Hydrology*, *613*, 128385. https://doi.org/10.1016/j.jhydrol.2022.128385

Littell, J. S., Peterson, D. L., Riley, K. L., Liu, Y., & Luce, C. H. (2016). A review of the relationships between drought and forest fire in the United States. *Global Change Biology*, *22*(7), 2353–2369. https://doi.org/10.1111/gcb.13275

Lloyd-Hughes, B. (2012). A spatio-temporal structure-based approach to drought characterisation. *International Journal of Climatology*, *32*(3), 406–418. https://doi.org/10.1002/joc.2280

Lloyd-Hughes, B., & Saunders, M. A. (2002). A drought climatology for Europe. *International Journal of Climatology*, *22*(13), 1571–1592. https://doi.org/10.1002/joc.846

Luo, M., Wu, S., Lau, G. N.-C., Pei, T., Liu, Z., Wang, X., Ning, G., Chan, T. O., Yang, Y., & Zhang, W. (2024). Anthropogenic forcing has increased the risk of longer-traveling and slower-moving large contiguous heatwaves. *Science Advances*, *10*(13), eadl1598. https://doi.org/10.1126/sciadv.adl1598

Maraun, D., Shepherd, T. G., Widmann, M., Zappa, G., Walton, D., Gutiérrez, J. M., Hagemann, S., Richter, I., Soares, P. M. M., Hall, A., & Mearns, L. O. (2017). Towards process-informed bias correction of climate change simulations. *Nature Climate Change*, *7*(11), 764–773. https://doi.org/10.1038/nclimate3418

Marson, P., Corre, L., Soubeyroux, J.-M., Sauquet, E., Robin, Y., Vrac, M., & Dubois, C. (2024, January 24). *Rapport de synthese sur les projections climatiques regionalisees*. EXPLORE2.

McKee, T. B., Doesken, N. J., & Kleist, J. (1993). THE RELATIONSHIP OF DROUGHT FREQUENCY AND DURATION TO TIME SCALES. *Eighth Conference on Applied Climatology*.

Najac, J., Kitova, N., Vidal, J.-P., Soubeyroux, J.-M., & Martin, E. (2010). Caractérisation des sécheresses en France au cours du XXIe siècle. *XXIIIe Colloque de l'Association Internationale de Climatologie. Risques et Changement Climatique*, p. 433 –p. 438. Retrieved April 9, 2024, from https://hal.science/hal-00536859

Naveau, P., Huser, R., Ribereau, P., & Hannart, A. (2016). Modeling jointly low, moderate, and heavy rainfall intensities without a threshold selection. *Water Resources Research*, *52*(4), 2753–2769. https://doi.org/10.1002/2015WR018552

Palmer, W. C. (1965). *Meteorological Drought*. U.S. Department of Commerce, Weather Bureau.

Piao, S., Friedlingstein, P., Ciais, P., de Noblet-Ducoudré, N., Labat, D., & Zaehle, S. (2007). Changes in climate and land use have a larger direct impact than rising CO2 on global river runoff trends. *Proceedings of the National Academy of Sciences*, *104*(39), 15242–15247. https://doi.org/10.1073/pnas.0707213104

Pieper, P., Düsterhus, A., & Baehr, J. (2020). A universal Standardized Precipitation Index candidate distribution function for observations and simulations. *Hydrology and Earth System Sciences*, *24*(9), 4541–4565. https://doi.org/10.5194/hess-24-4541-2020

Raza, A., Al-Ansari, N., Hu, Y., Acharki, S., Vishwakarma, D. K., Aghelpour, P., Zubair, M., Wandolo, C. A., & Elbeltagi, A. (2022). Misconceptions of Reference and Potential

Evapotranspiration: A PRISMA-Guided Comprehensive Review. *Hydrology*, *9*(9), 153. https://doi.org/10.3390/hydrology9090153

Ribes, A., Boé, J., Qasmi, S., Dubuisson, B., Douville, H., & Terray, L. (2022). An updated assessment of past and future warming over France based on a regional observational constraint. *Earth System Dynamics*, *13*(4), 1397–1415. https://doi.org/10.5194/esd-13-1397-2022

Robin, Y., Corre, L., Marson, P., Bernus, S., Vrac, M., & Thao, S. (2023, March 9). *Projections climatiques régionalisées : Correction de biais et changements futurs*. EXPLORE2.

Roudier, P., Andersson, J. C. M., Donnelly, C., Feyen, L., Greuell, W., & Ludwig, F. (2016). Projections of future floods and hydrological droughts in Europe under a +2°C global warming. *Climatic Change*, *135*(2), 341–355. https://doi.org/10.1007/s10584-015-1570-4

Sauquet, E., Thirel, G., Vergnes, J.-P., & Habets, F. (2022, August 31). *Etude d'impact du changement climatique sur le regime hydrologique en france metropolitaine – synthese bibliographique*. EXPLORE2.

Sauquet, É., Héraut, L., Bonneau, J., Reverdy, A., Strohmenger, L., & Vidal, J.-P. (2023, December 12). *Diagnostic des modèles hydrologiques : des données aux résultats.*

Seneviratne, S. I., Zhang, X., Adnan, M., Badi, W., Dereczynski, C., Di Luca, A., Ghosh, S., Iskander, I., Kossin, J., Lewis, S., Otto, F., Pinto, I., Satoh, M., Vicente-Serrano, S. M., Wehner, M., & Zhou, B. (with Greve, P.). (2021). Weather and climate extreme events in a changing climate (chapter 11). In V. Masson-Delmotte, P. Zhai, A. Pirani, S. L. Connors, C. Péan, S. Berger, N. Caud, Y. Chen, L. Goldfarb, M. I. Gomis, M. Huang, K. Leitzell, E. Lonnoy, J. B. R. Matthews, T. K. Maycock, T. Waterfield, K. Yelekçi, R. Yu, & B. Zhu (Eds.). Cambridge University Press. Retrieved April 9, 2024, from https://www.ipcc.ch/report/ar6/wg1/

Shepherd, T. G. (2016). A Common Framework for Approaches to Extreme Event Attribution. *Current Climate Change Reports*, *2*(1), 28–38. https://doi.org/10.1007/s40641-016-0033-y

Shepherd, T. G. (2019). Storyline approach to the construction of regional climate change information. *Proceedings of the Royal Society A: Mathematical, Physical and Engineering Sciences*, *475*(2225), 20190013. https://doi.org/10.1098/rspa.2019.0013

Shepherd, T. G., Boyd, E., Calel, R. A., Chapman, S. C., Dessai, S., Dima-West, I. M., Fowler, H. J., James, R., Maraun, D., Martius, O., Senior, C. A., Sobel, A. H., Stainforth, D. A., Tett, S. F. B., Trenberth, K. E., van den Hurk, B. J. J. M., Watkins, N. W., Wilby, R. L., & Zenghelis, D. A. (2018). Storylines: An alternative approach to representing uncertainty in physical aspects of climate change. *Climatic Change*, *151*(3), 555–571. https://doi.org/10.1007/s10584-018-2317-9

Sillmann, J., Shepherd, T. G., van den Hurk, B., Hazeleger, W., Martius, O., Slingo, J., & Zscheischler, J. (2021). Event-Based Storylines to Address Climate Risk. *Earth's Future*, *9*(2), e2020EF001783. https://doi.org/10.1029/2020EF001783

Taylor, K. E., Stouffer, R. J., & Meehl, G. A. (2012). An Overview of CMIP5 and the Experiment Design. *Bulletin of the American Meteorological Society*, *93*(4), 485–498. https://doi.org/10.1175/BAMS-D-11-00094.1

Tramblay, Y., Sauquet, E., Arnaud, P., Rousset, F., Soubeyroux, J.-M., Jeantet, A., Munier, S., & Vergnes, J.-P. (2024, June 28). *Scenarios d'extremes hydrologiques*. EXPLORE2.

Van Loon, A. F., Gleeson, T., Clark, J., Van Dijk, A. I. J. M., Stahl, K., Hannaford, J., Di Baldassarre, G., Teuling, A. J., Tallaksen, L. M., Uijlenhoet, R., Hannah, D. M., Sheffield, J., Svoboda, M., Verbeiren, B., Wagener, T., Rangecroft, S., Wanders, N., &

Van Lanen, H. A. J. (2016). Drought in the Anthropocene. *Nature Geoscience*, *9*(2), 89–91. https://doi.org/10.1038/ngeo2646

Van Loon, A. F., Stahl, K., Di Baldassarre, G., Clark, J., Rangecroft, S., Wanders, N., Gleeson, T., Van Dijk, A. I. J. M., Tallaksen, L. M., Hannaford, J., Uijlenhoet, R., Teuling, A. J., Hannah, D. M., Sheffield, J., Svoboda, M., Verbeiren, B., Wagener, T., & Van Lanen, H. A. J. (2016). Drought in a human-modified world: Reframing drought definitions, understanding, and analysis approaches. *Hydrology and Earth System Sciences*, *20*(9), 3631–3650. https://doi.org/10.5194/hess-20-3631-2016

van Vuuren, D. P., Edmonds, J., Kainuma, M., Riahi, K., Thomson, A., Hibbard, K., Hurtt, G. C., Kram, T., Krey, V., Lamarque, J.-F., Masui, T., Meinshausen, M., Nakicenovic, N., Smith, S. J., & Rose, S. K. (2011). The representative concentration pathways: An overview. *Climatic Change*, *109*(1), 5. https://doi.org/10.1007/s10584-011-0148-z

Vautard, R., Kadygrov, N., Iles, C., Boberg, F., Buonomo, E., Bülow, K., Coppola, E., Corre, L., van Meijgaard, E., Nogherotto, R., Sandstad, M., Schwingshackl, C., Somot, S., Aalbers, E., Christensen, O. B., Ciarlo, J. M., Demory, M.-E., Giorgi, F., Jacob, D., . . . Wulfmeyer, V. (2021). Evaluation of the Large EURO-CORDEX Regional Climate Model Ensemble. *Journal of Geophysical Research: Atmospheres*, *126*(17), e2019JD032344. https://doi.org/10.1029/2019JD032344

Verfaillie, D., Déqué, M., Morin, S., & Lafaysse, M. (2017). The method ADAMONT v1.0 for statistical adjustment of climate projections applicable to energy balance land surface models. *Geoscientific Model Development*, *10*(11), 4257–4283. https://doi.org/10.5194/gmd-10-4257-2017

Vernay, M., Lafaysse, M., Monteiro, D., Hagenmuller, P., Nheili, R., Samacoïts, R., Verfaillie, D., & Morin, S. (2022). The S2M meteorological and snow cover reanalysis over the French mountainous areas: Description and evaluation (1958–2021). *Earth System Science Data*, *14*(4), 1707–1733. https://doi.org/10.5194/essd-14-1707-2022

Vicente-Serrano, S. M., Beguería, S., & López-Moreno, J. I. (2010). A Multiscalar Drought Index Sensitive to Global Warming: The Standardized Precipitation Evapotranspiration Index. *Journal of Climate*, *23*(7), 1696–1718. https://doi.org/10.1175/2009JCLI2909.1

Vidal, J.-P., Martin, E., Franchistéguy, L., Baillon, M., & Soubeyroux, J.-M. (2010). A 50-year high-resolution atmospheric reanalysis over France with the Safran system. *International Journal of Climatology*, *30*(11), P. 1627. https://doi.org/10.1002/joc.2003

Vidal, J.-P., Martin, E., Franchistéguy, L., Habets, F., Soubeyroux, J.-M., Blanchard, M., & Baillon, M. (2010). Multilevel and multiscale drought reanalysis over France with the Safran-Isba-Modcou hydrometeorological suite. *Hydrology and Earth System Sciences*, *14*(3), 459–478. https://doi.org/10.5194/hess-14-459-2010

Vidal, J.-P., Martin, E., Kitova, N., Najac, J., & Soubeyroux, J.-M. (2012). Evolution of spatio-temporal drought characteristics: Validation, projections and effect of adaptation scenarios. *Hydrology and Earth System Sciences*, *16*(8), 2935–2955. https://doi.org/10.5194/hess-16-2935-2012

Vogel, M. M., Zscheischler, J., Fischer, E. M., & Seneviratne, S. I. (2020). Development of Future Heatwaves for Different Hazard Thresholds. *Journal of Geophysical Research: Atmospheres*, *125*(9), e2019JD032070. https://doi.org/10.1029/2019JD032070

Wilhite, D. A. (2016, September 17). *Droughts: A global assesment*. Routledge.

Wilhite, D. A., & Glantz, M. H. (1985). Understanding the drought phenomenon: The role of definitions. *Water International*. https://doi.org/10.1080/02508068508686328

Zargar, A., Sadiq, R., Naser, B., & Khan, F. I. (2011). A review of drought indices. *Environmental Reviews*, *19*, 333–349. https://doi.org/10.1139/a11-013

Zscheischler, J., Mahecha, M. D., Harmeling, S., & Reichstein, M. (2013). Detection and attribution of large spatiotemporal extreme events in Earth observation data. *Ecological Informatics*, *15*, 66–73. https://doi.org/10.1016/j.ecoinf.2013.03.004

Zscheischler, J., Reichstein, M., von Buttlar, J., Mu, M., Randerson, J. T., & Mahecha, M. D. (2014). Carbon cycle extremes during the 21st century in CMIP5 models: Future evolution and attribution to climatic drivers. *Geophysical Research Letters*, *41*(24), 8853–8861. https://doi.org/10.1002/2014GL062409

A. EXPLORE2 Models

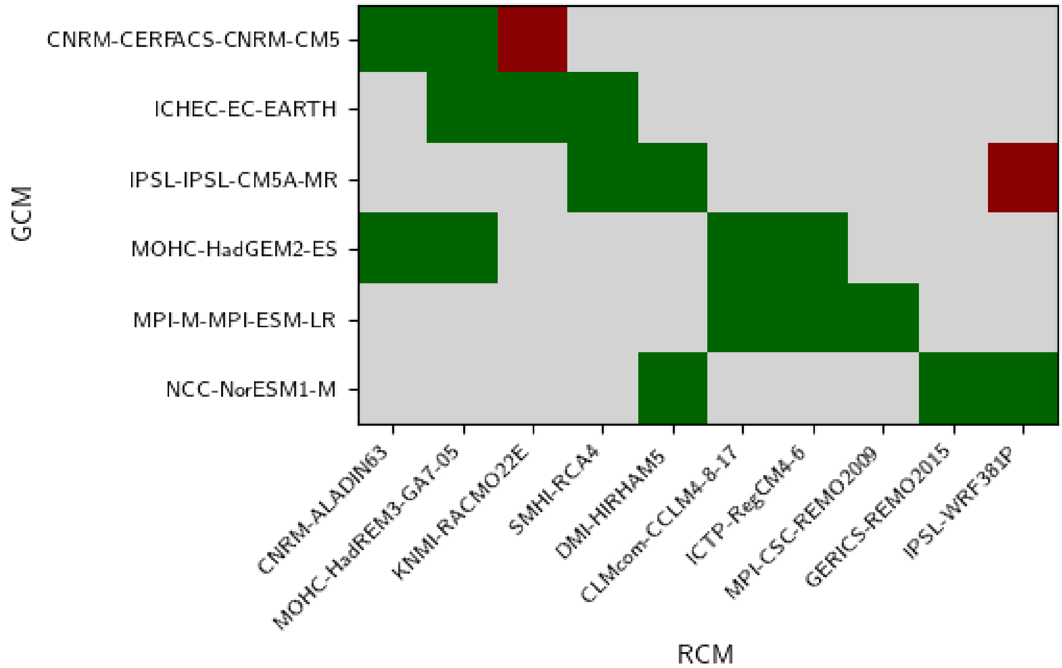

Figure A.1 – The RCM-GCM couples used in the EXPLORE2 simulations are indicated by green shading. The couples with red shading were excluded from the EXPLORE2 ensemble (Marson et al., 2024).

B. EXPLORE2 Storylines

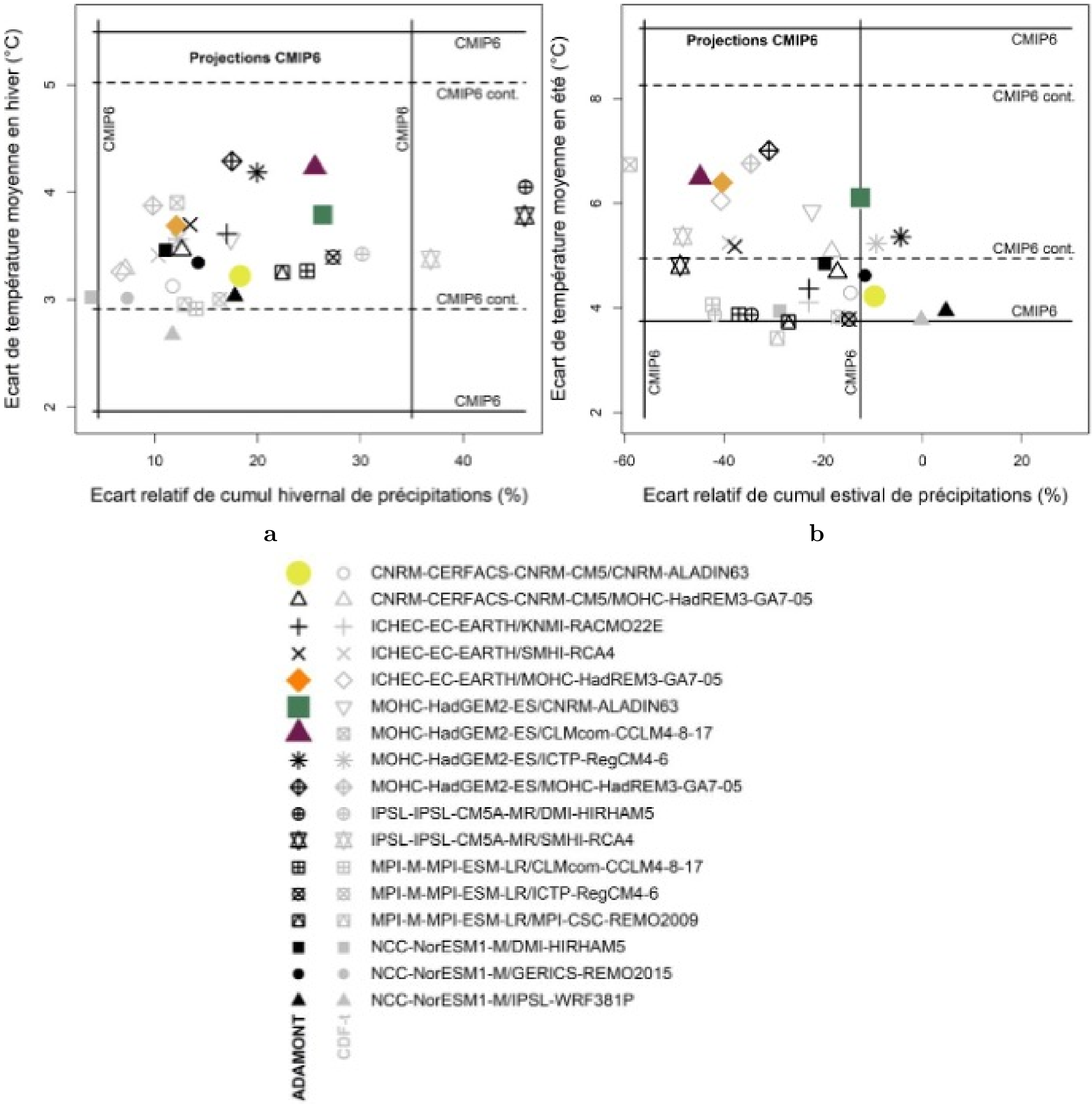

Figure B.1 – Projected relative changes in France for (a) winter and (b) summer temperatures (y axis) and precipitation (x axis) of the EXPLORE2 simulations and the four storylines. The simulations are compared with the 5% and 95% quantiles (Q5 and Q95) of the CMIP6 ensemble, which is represented by the plain lines, and CMIP6 constrained by temperature observations according to the method of Ribes et al., 2022, which is represented by the dashed lines (Marson et al., 2024).

Marson et al., 2024 described the four storylines as follow.

The green storyline indicated that the temperature in France reached 4.8°C above the climatology, exhibiting pronounced seasonal contrasts. The temperature in winter was recorded at +3.8°C, while in summer it reached +6.1°C. The mean precipitation level increased by six percent. This upward trend can be attributed to a notable increase in winter precipitation (+26%), particularly evident in the northern half of the country. This increase was not offset by a moderate and insignificant decrease in summer precipitation (-13%). Additionally, changes in maximum precipitation have been observed to increase (+25%). In response to warming, reference evapotranspiration has increased (+31%) and has exceeded the rise in precipitation, resulting in a decrease in the water balance (approximately -160%).

The yellow storyline indicated that the observed warming of +3.7°C did not exceed the +4°C threshold across France, with moderate seasonal contrasts. The winter temperature was +3.2°C, while the summer temperature was +4.2°C. The mean precipitation level increased by six percent. This upward trend can be attributed to a notable increase in precipitation during the winter season (+18%) in the northern half of the country, which was not counterbalanced by a moderate reduction in summer precipitation (-10%). This latter reduction was not significant in the large north-eastern quarter. The greatest changes in precipitation are occurring in the northern half of the country, with an increase of 16%. In response to warming, reference evapotranspiration has increased by 28%, which outweighs the rise in precipitation. This has resulted in a decrease in the water balance of approximately 150%.

The orange storyline exhibited a warming trend of +4.6°C across France, with pronounced seasonal contrasts. During the winter period, the temperature increase was relatively modest (+3.7°C), while in the summer, it reached +6.4°C, demonstrating a notable intensification. The mean precipitation level exhibited a decline of 9%. This downward trend can be attributed to a pronounced drying-up during the summer months (40%), particularly evident in the southern half of the country. This was not compensated for by the moderate increase in precipitation during the winter (+12%), which was insignificant outside the north-eastern quarter. The observed changes in maximum precipitation are relatively minor, with an increase of 12%. However, in response to warming, there has been a notable rise in reference evapotranspiration, reaching 43%. When coupled with the decline in precipitation, this has resulted in a significant reduction in the water balance, with a deficit of nearly 400%.

The purple storyline indicated that temperatures in France reached 5°C above the seasonal norm, exhibiting pronounced seasonal contrasts. The mean temperature in winter was +4.2°C, while in summer it was +6.5°C. The mean precipitation level exhibited a decline of approximately 8%. This trend conceals pronounced seasonal contrasts, with a notable drying out during the summer months (-45%), particularly evident in the southern regions, which outweighs the increase in precipitation during the winter (+21%), predominantly affecting the northern half of the country. The observed changes in maximum precipitation are insignificant in the southernmost regions, with an increase of only 26%. In response to warming, there has been a notable increase in reference evapotranspiration (+26%). When considered alongside the decline in precipitation, this results in a significant reduction in the water balance, estimated to be approximately -230%.

C. Potential Evapotranspiration

Potential evapotranspiration (PET) is defined as the maximum amount of water that could be evaporated and transpired. It represents the atmospheric demand for moisture and can be calculated using a variety of formulae. The one employed in this analysis is a combination of the Penman-Monteith equation and the Hargreaves formula.

The Penman-Monteith equation is a widely used model for estimating PET, combining physical principles of energy balance and mass transfer. This method considered factors such as net radiation, temperature, wind speed, and humidity, providing a comprehensive approach to PET estimation. The equation is as follows:

$$\mathrm{PET} = \frac{0.408\Delta(R_n - G) + \gamma\frac{900}{T+273}u_2(e_s - e_a)}{\Delta + \gamma(1 + 0.34u_2)} \tag{C.1}$$

Where:

- Δ is the slope of the saturation vapor pressure curve (kPa/°C),
- R_n is the net radiation at the crop surface (MJ/m^2/day),
- G is the soil heat flux density (MJ/m^2/day),
- γ is the psychrometric constant (kPa/°C),
- T is the mean daily air temperature (°C),
- u_2 is the wind speed at 2 meters height (m/s),
- e_s is the saturation vapor pressure (kPa),
- e_a is the actual vapor pressure (kPa).

This equation is widely adopted due to its physical basis. The first part of the equation describes the process of evaporation, while the second part describes the process of convection. However, this equation requires a significant number of meteorological data inputs (Allen, 2000).

In contrast, the Hargreaves formula provided a simpler approach to estimating PET. The formula was given as:

$$\mathrm{PET} = 0.0023(T_{max} - T_{min})^{0.5}(T_{mean} + 17.8)R_a \tag{C.2}$$

Where:

- T_{max} and T_{min} are the maximum and minimum temperatures (°C),
- $T_{mean}$is the mean temperature (°C),
- R_a is the extraterrestrial radiation (MJ/m^2/day).

Although the Hargreaves formula is less precise than the Penman-Monteith equation, it is appreciated for its simplicity and minimal data requirements, which make it a practical choice for use in diverse environmental conditions (Hargreaves and Samani, 1985).

In the Hargreaves Formula, the solar radiation is estimated from the air temperature. In the EXPLORE2 project, the net radiation from the Hargreaves Formula, noted $R_n^{Hargreaves}$, is used in the Penman-Monteith equation, which yields the formula of Equation C.3.

$$\mathrm{PET} = \frac{0.408\Delta(R_n^{Hargreaves} - G) + \gamma\frac{900}{T+273}u_2(e_s - e_a)}{\Delta + \gamma(1 + 0.34u_2)} \tag{C.3}$$